Multi-scale interactions between turbulence and magnetic islands and parity mixture-a review

Ishizawa, A; Kishimoto, Y; Nakamura, Y

Plasma Physics and Controlled Fusion

PAPER • **OPEN ACCESS**

Multi-scale interactions between turbulence and magnetic islands and parity mixture—a review

To cite this article: A Ishizawa *et al* 2019 *Plasma Phys. Control. Fusion* **61** 054006

OPEN ACCESS
IOP Publishing
Plasma Physics and Controlled Fusion
Plasma Phys. Control. Fusion **61** (2019) 054006 (22pp)
https://doi.org/10.1088/1361-6587/ab06a8

Multi-scale interactions between turbulence and magnetic islands and parity mixture—a review

A Ishizawa, Y Kishimoto and Y Nakamura

Graduate School of Energy Science, Kyoto University, Uji, Kyoto 611-0011, Japan

E-mail: ishizawa@energy.kyoto-u.ac.jp

Received 29 September 2018, revised 12 December 2018
Accepted for publication 12 February 2019
Published 26 March 2019

Abstract

This paper presents a review of multi-scale interactions between small-scale turbulence and large scale magnetic islands. In finite beta plasmas, zonal flows are relatively weak, and thus another electromagnetic coherent structure formation such as magnetic islands becomes important for regulating turbulence. In multi-scale interactions, large-scale modes dominate turbulent fluctuations even when the growth rate of the large-scale mode is much smaller than small-scale modes. On the other hand, small-scale modes influence large-scale modes when the large-scale modes are stable/marginally stable. Thus, the multi-scale interactions are categorized according to the stability of tearing mode (TM), which drives large-scale magnetic islands. When the TM is unstable, wide magnetic islands are produced, and as a result of the multi-scale interactions, the turbulent transport is significantly enhanced inside the separatrix of the island, because large-scale stable modes are excited by mutual interactions between turbulence and the island. On the other hand, a steep temperature gradient is formed around the separatrix of the island, which is consistent with zonal flow shear appearing at the separatrix. When the TM is stable/marginally stable, turbulence drives and sustains magnetic islands of width equal to multiples of the Larmor radius. This excitation of islands by turbulence can be related to the seed island formation of neo-classical TMs. The parity of fluctuations plays crucial role in the multi-scale nonlinear interactions, because pure twisting parity mode does not satisfy the nonlinear fluid/gyrokinetic equations. Magnetic islands belongs to the tearing parity mode and drift-wave instabilities normally belong to the twisting parity mode, and each parity is conserved in the linear growth of the instability. However, when the amplitude of the twisting parity mode becomes finite, the nonlinear energy transfer takes place from the twisting parity to tearing parity modes. Through this nonlinear parity mixture, the magnetic islands are produced by the turbulence. The influence of anomalous current drive and polarization current on the multi-scale interactions is discussed as well.

Keywords: turbulence, magnetic island, multi-scale, parity, numerical simulation

(Some figures may appear in colour only in the online journal)

1. Introduction

Turbulence is considered to cause anomalous transport in magnetically confined plasmas [1–3], and is mainly driven by drift-wave instabilities such as ion-temperature-gradient (ITG) mode and trapped electron mode (TEM). The drift-wave turbulence produces zonal flows through nonlinearity, then the turbulence is regulated by the zonal flows at low β [4]. When the normalized pressure β becomes finite, turbulent fluctuations becomes electromagnetic [5–7], and magnetic perturbations play important role in the turbulent transport. At finite beta, the fluctuations of the ITG mode become electromagnetic and

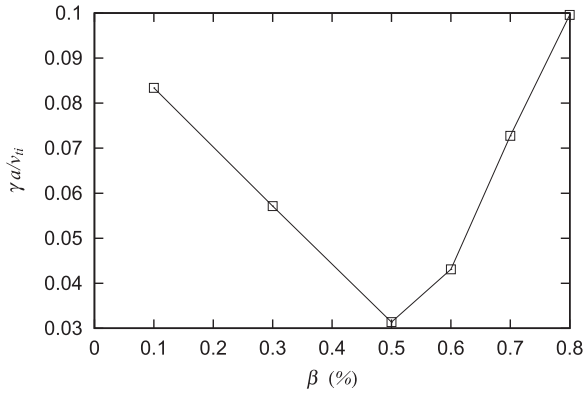

Figure 1. Plasma beta dependence of linear growth rate calculated from a two-fluid model (five-field model) described in section 2. The ITG mode is unstable at low β and the KBM is destabilized at high β. Reproduced courtesy of IAEA. Figure from [8]. Copyright 2007 IAEA.

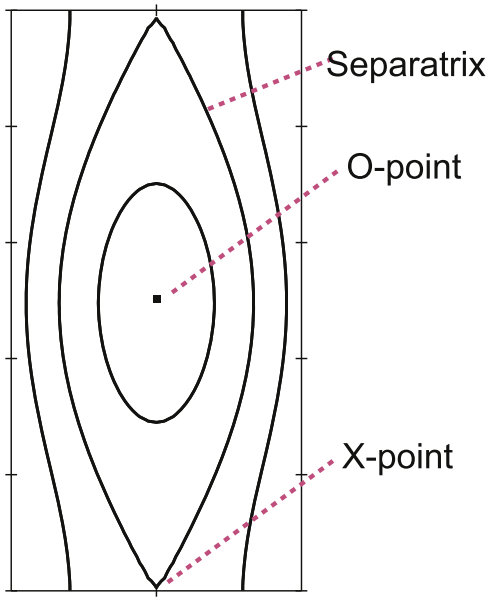

Figure 2. A magnetic island.

kinetic ballooning mode (KBM) can be destabilized at high β (figure 1) [8]. In addition, electromagnetic fluctuations give rise to a long wavelength MHD instability such as tearing modes (TMs) which reconnect the closed magnetic surfaces and degrade the confinement. In the finite β plasma zonal flows become weak so that coherent structure formation rather than the zonal flow production can be a mechanism controlling turbulent transport. Especially, coherent magnetic islands that have a long wavenumber play an important role as well as the zonal magnetic field and zonal pressure field.

Magnetic islands are represented by the Poincare map of magnetic field lines on a cross-section of torus. The map forms curved lines, which are cross sections of the good flux surfaces (figure 2). The field lines have a concentric structure surrounding a point called O-point, where the component of

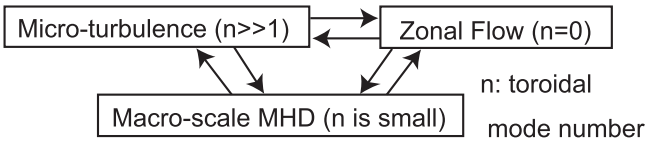

Figure 3. Schematic drawing of multiscale interactions. Reprinted from [25], with the permission of AIP Publishing.

magnetic field on the cross-section vanishes. Another vanishing point of the field is called X-point, which is a stagnation point of the field line. The line goes through the X-point is called as the separatrix of magnetic island. Since the parallel streaming of particles is fast in magnetically confined plasmas, the profiles of temperature and density tend to flatten inside the separatrix of the island resulting in the degradation of confinement [9], and thus the appearance of magnetic islands can limit the performance of tokamak plasmas such as the standard ELMy H-mode and advanced scenarios of ITER [10]. Furthermore, when coherent magnetic island chains appearing at different radii become wide and overlap each other, the degradation of confinement is significant and a disruption terminates the discharge of tokamak plasma [10]. This is because the overlap of coherent magnetic islands results in stochastic magnetic field in wide range of radius, and then flattening of temperature and density profiles is significantly enhanced.

When a plasma is confined by a set of nested magnetic surfaces, magnetic islands are produced by magnetic reconnection, which changes the topology of magnetic field lines and violates the nested surfaces. The point where the reconnection takes place is the X-point. Magnetic islands are caused by TMs, which is a spontaneous magnetic reconnection [11]. Neoclassical tearing mode (NTM) produces magnetic islands at a low-order rational surface and is one of primary instabilities limiting the achievable plasma pressure of high-β tokamak plasmas. NTMs are nonlinear MHD instabilities due to the perturbed bootstrap current caused by pressure flattening inside the separatrix of magnetic island, and thus they start to grow from finite size magnetic islands required for overcoming a threshold of destabilization [12]. The typical width of this seed magnetic island is evaluated to be several times as large as the ion Larmor radius from experimental data [13]. The seed island can be excited by another MHD activity such as a sawtooth crash and edge localized modes (ELMs). For instance, a sawtooth crash, which has $(m, n) = (1, 1)$ fluctuation, excites an higher harmonics $(m, n) = (2, 2)$ at $q = 1$ rational surface, and then generates $(m, n) = (3, 2)$ magnetic perturbation because of the toroidal geometry. This $(m, n) = (3, 2)$ magnetic perturbation produces seed magnetic islands and then excites an NTM at $q = 3/2$ rational surface. On the other hand, an $(m, n) = (2, 1)$ NTM is observed without any sawtooth crashes and ELMs in the JT-60U experiments [14]. Thus, the electromagnetic drift-wave turbulence can be a candidate for explanation of this experimental observation on the excitation of NTM without MHD activities. Magnetic islands are also produced by magnetic reconnection caused by externally applied resonant magnetic perturbations (RMPs) at a rational

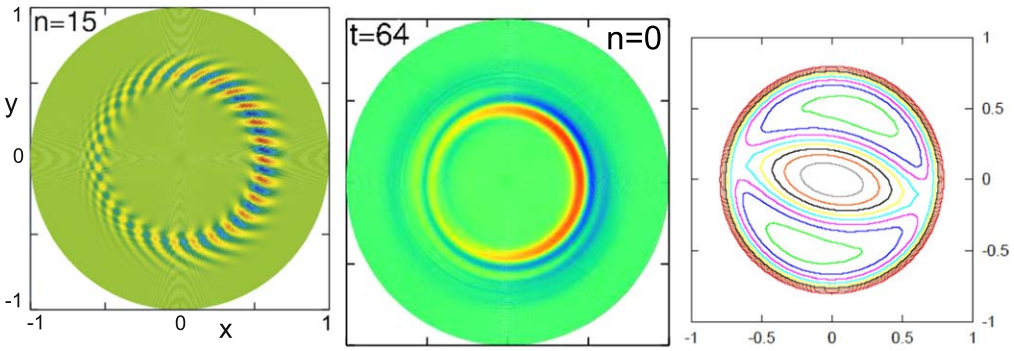

Figure 4. Color map of electrostatic potential on a poloidal section for drift-wave instability with $n = 15$ and zonal flow $n = 0$, and magnetic field lines of $(m, n) = (2, 1)$ magnetic islands on a poloidal section. Reproduced courtesy of IAEA. Figure from [30]. Copyright 2009 IAEA.

Table 1. The stability parameter of tearing mode Δ' in numerical simulations.

Stability of tearing mode	Stable–unstable	Marginally stable–unstable	Unstable
References	[37]	[39, 47, 51–53]	[43, 49]
Stability parameter Δ'	−3.4 to 1.8	−0.45 to 1.2	3.0

surface in the edge region. The RMPs are used to control the ELMs [15], which is expected to appear in the standard ELMy H-mode of ITER, by violating the nested magnetic surfaces at the edge region. The island formation by RMPs can be influenced by strong $E \times B$ flow and by edge turbulence, which can be an electromagnetic drift-wave turbulence.

Nonlinear interactions between turbulence and coherent modes, which can be magnetic islands and long lasting modes, become an important issue in understanding the mechanism of confinement degradation, because drift-wave turbulence is ubiquitous in magnetically confined plasmas, and nonlinearly interacts with magnetic island. In fact, low-wavenumber MHD activities are observed before the disruption in reversed shear plasmas with a transport barrier related to zonal flows and drift-wave turbulence in JT-60U [16]. In addition, micro turbulence is observed in LHD plasmas that usually exhibit MHD activities [17]. The interaction between turbulence and magnetic islands is a multi-scale (cross-scale) interaction illustrated in figure 3. The turbulence is driven by drift-wave instability characterized by high toroidal wavenumber $n \gg 1$ (figure 4), while the magnetic islands can be caused by TM characterized by low toroidal wavenumber $n \sim 1$ (figure 4). Thus, this multi-scale interaction originates from a high wavenumber nature of the pressure driven instability and a low wavenumber nature of the current driven instability. Theoretical study on interactions between turbulence and magnetic islands mainly focuses on the influence of turbulence on the growth of TM through anomalous resistivity, anomalous electron viscosity, and negative viscosity due to turbulence [18–23]. Mutual interactions between turbulence and magnetic islands are studied numerically by means of fluid model [8, 24–54]and by gyrokinetic model [55–63], and they are reviewed in this paper. Since magnetic islands are generated by TMs, which are a long wavelength MHD instability mainly driven by an equilibrium current density gradient, it is convenient to separately discuss two cases: the TM is unstable and stable. When the TM is unstable we have magnetic islands which are much wider than the ion Larmor radius $W \gg \rho_i$ [8, 24–27, 29, 30, 34, 35, 40, 43, 48, 49] as will be discussed in section 4. On the other hand, when TM is stable [37, 54] or marginally stable [39, 44, 47, 51–53] turbulence produces magnetic islands with $W \geqslant \rho_i$ as will be discussed in section 5. In addition, static magnetic islands interacting with turbulence is investigated to elucidate the influence of magnetic islands on turbulence and polarization current effects [28, 31–33, 36, 38, 41, 42, 45, 46, 50] as will be discussed in section 6. The TM stability parameters Δ' [11] of numerical simulations are listed in table 1.

Recently, experimental observation of the interactions between turbulent fluctuations and magnetic islands have been extensively studied [64–73]. The spatial correlation between turbulent electron temperature fluctuations and magnetic islands in KSTAR is reported [67]. The relation between turbulent density fluctuation and a magnetic island in DIII-D is presented [68, 69]. The temporal correlations between turbulence and magnetic islands in HL-2A and EAST are investigated [70–73]. Comparison with numerical simulation results has just started.

Multi-scale interactions causing the appearance of magnetic island in quasi-steady turbulent state including zonal flows, and geodesic acoustic mode (GAM) in a torus plasma is firstly presented by two-fluid simulations [25]. Then, it is demonstrated that multi-scale interactions between turbulence and magnetic islands have significant impact on the turbulent transport at finite beta as shown in flux-driven electromagnetic two-fluid simulations [30]. The mechanisms of interactions are extensively studied by simplifying geometry of plasmas such as cylindrical [24, 45, 47] or slab plasmas [28, 29, 31, 34, 35, 37, 39, 42, 44, 50–54] (tables 2 and 3).

When the TM is unstable, large magnetic islands $W \gg \rho_i$ are produced by the instability. Then magnetic islands influence turbulence by magnetic perturbations, by producing coherent vortex flows, and by pressure flattening (section 4). The flattening of temperature and density profiles inside the separatrix of the magnetic island is incomplete because of the penetration of turbulence inside the separatrix. That is observed in many

Table 2. Fluid models and plasma geometry used for studies of multi-scale interactions between small-scale turbulence and large-scale magnetic islands, where EM, ES, and flux-driven represent electromagnetic, electrostatic and flux-driven simulations, respectively. Each model can describe several instabilities which are toroidal ITG mode (tITG), kinetic ballooning mode (KBM), tearing mode (TM), internal kink mode (IK), interchange mode (IC), and slab ITG mode (sITG). Turbulence is driven by the instability typed by bold letter in the paper labeled by the name of first author.

	Five-field (ϕ, ψ, n, $v_\parallel$, T_i)	Four-field (ϕ, ψ, n, $v_\parallel$)	Three-field (ϕ, ψ, n)	Three-field (n, $v_\parallel$, $T_\parallel$)
Flux driven Torus, EM	tITG, **KBM**, GAM, TM, IK Ishizawa [30]			
Torus, EM	tITG, **KBM**, GAM, TM, IK Ishizawa [8, 25]			
Cylinder, EM		**IC**, TM, IK Yagi [24]	**IC**, TM Poye [47]	
Cylinder, ES				**sITG** Hariri [45]
Slab, EM	**sITG**, IC, TM Li [29, 40], Ishizawa [37] Hu [43, 48], Liu [49]	**IC**, TM Sato [54]	**IC**, TM Muraglia [34, 35, 39, 53] Agullo [44, 51, 52]	
Slab, ES	**sITG**, IC Ishizawa [42], Izacard [50]		**IC** Militello [28] Waelbroeck [31]	**sITG** Hill [46]

Table 3. Gyrokinetic simulations for the interactions between turbulence and magnetic islands.

	ES, static island	EM, static island	EM, $\Delta' > 0$
References	[55–57, 63]	[59, 60]	[61, 62]

simulations and experiments (section 4.1) [30, 44–46, 55, 57, 69]. The enhancement of turbulent transport inside the separatrix is attributed to coherent vortex flows produced by interactions between the turbulence and magnetic islands (section 4.2) [8, 25, 36, 55, 57, 59]. The poloidal angle dependence of turbulence intensity caused by magnetic islands is weak in flux-driven simulations [30], while it is strong in non-flux-driven simulations [32, 57]. Zonal flows are not strong in electromagentic turbulence at finite β, furthermore the flows are modified by magnetic islands because of the violated magnetic surfaces [30, 63]. In addition, zonal flows oscillate by the presence of magnetic islands (section 4.3) [29, 40, 59]. Magnetic field lines can be stochastic in torus plasma, and the X-point is sensitive to magnetic perturbations, and thus magnetic fluctuations of turbulence enhance the stochasticity of magnetic field lines around the separatrix including the X-points of magnetic islands (section 4.4) [30, 61]. The turbulence influences magnetic islands when they are small and growing, and the growth of magnetic islands is enhanced by turbulent anomalous resistivity (section 4.5) [27, 40, 50].

When TMs are stable, turbulence produces long wavelength magnetic islands with small width $W \geqslant \rho_i$ (section 5) [37, 39, 47, 52, 53, 61, 62], because turbulent fluctuations become electromagnetic at finite β. This issue is linked to the excitation of NTMs [12, 13, 74], which limit the achievable β of tokamak plasmas, because the turbulence can produce the seed island of NTMs that appears even if the conventional TM is stable. The process of magnetic island formation by turbulence is not simple. The nonlinear mode coupling between large scale coherent mode with small scale turbulence can generally exist, so that a large-scale mode can be excited. However, this does not mean the excitation of magnetic islands, because the magnetic islands appear only when magnetic reconnection takes place and the topology of magnetic field lines is changed on the low (m, n) rational surface where the magnetic field line bending stabilizing effect is weak [25]. Thus, in addition to the energy transfer to a coherent mode, the parity mixture and magnetic reconnection are required for the formation of magnetic islands.

In addition to the categorization based on the stability of TMs, it is useful to study turbulence in a static magnetic island (section 6), because the polarization current effect, which is one of the important mechanisms of magnetic island growth, is evaluated by using the static island model. The polarization current due to turbulence is firstly investigated by numerical simulations for electrostatic interchange modes (ICs) [28, 31], and then it is studied by simulations for ITG turbulence [42]. It is found that the polarization current due to turbulence can drive magnetic islands [31, 42].

The organization of the remainder of the paper is as follows. Fluid models used in numerical simulations are described in section 2. The parity symmetry is explained in section 3. The multi-scale interactions when the TM is unstable is presented in section 4. Then, the interactions when the TM is stable is described, and the importance of parity is demonstrated in section 5. The analysis using a static magnetic island is described in section 6. Summary is given in section 7.

2. Model equations

Here, we describe two-fluid equations used in numerical simulations presented in this paper. Most of fluid models used for the study of interactions between turbulence and magnetic islands are a subset of the five-field model of two-fluid equations described here (table 2).

2.1. Fluid model used in simulations of toroidal plasma

We consider three-dimensional toroidal plasmas, and describe a reduced set of two-fluid equations that extends the standard reduced two-fluid equations [75] by including ion temperature with the Landau fluid closure [25, 76]. The model consists of the vorticity equation for the electrostatic potential ϕ, the electron density n equation, the parallel velocity $v_\parallel$ equation, the generalized Ohm's law for the magnetic flux function ψ, and the ion temperature T_i equation,

$$n_{\rm eq}\frac{D\nabla_\perp^2\phi}{Dt} = -\nabla_\parallel J - K[p] + \tilde{a}\nabla_\perp\cdot[\nabla_\perp\phi, p_i] + \mu\nabla_\perp^2\nabla_\perp^2\phi, \tag{1}$$

$$\frac{Dn}{Dt} = -n_{\rm eq}\nabla_\parallel v_{e\parallel} + K[n_{\rm eq}\phi - p_e] + \mu\nabla_\perp^2 n, \tag{2}$$

$$n_{\rm eq}\frac{Dv_\parallel}{Dt} = -\nabla_\parallel p + \mu\nabla_\perp^2 v_\parallel, \tag{3}$$

$$\beta\frac{\partial\psi}{\partial t} = -\nabla_\parallel\phi + \frac{1}{n_{\rm eq}}\nabla_\parallel p_e + \eta_L v_{e\parallel} + \eta J, \tag{4}$$

$$\frac{DT_i}{Dt} = -(\gamma-1)(T_{\rm eq}\nabla_\parallel v_\parallel + \kappa_L T_i) + T_{\rm eq}K[(\gamma-1)(\phi + T_i + T_{\rm eq}n/n_{\rm eq}) + \gamma T_i] + \mu\nabla_\perp^2 T_i, \tag{5}$$

where $\frac{Df}{Dt} = \frac{\partial f}{\partial t} + \tilde{a}[\phi, f]$, $\nabla_\parallel f = \epsilon\frac{\partial f}{\partial\zeta} - \beta\tilde{a}[\psi, f]$, $K[f] = 2\epsilon[r\cos\theta, f]$, $[f, g] = \frac{\partial f}{\partial r}\frac{\partial g}{r\partial\theta} - \frac{\partial f}{r\partial\theta}\frac{\partial g}{\partial r}$, $\eta_L = \sqrt{\frac{\pi}{2}\tau\frac{m_e}{m_i}}|\nabla_\parallel|$, $\kappa_L = \sqrt{\frac{8T_{\rm eq}}{\pi}}|\nabla_\parallel|$, where ρ_i, $\epsilon = a/R$, R, a and $\gamma = 5/3$, and $\tilde{a} = 1/\rho_* = a/\rho_i$, are the Larmor radius, the inverse of aspect ratio, the major radius, the minor radius, the specific heat, and the inverse of normalized Larmor radius. In these equations $J \equiv -J_\parallel = \nabla_\perp^2\psi$, $p = p_i + p_e$, $v_{e\parallel} = v_\parallel + J/n_{\rm eq}$, $p_i = nT_i$, $p_e = nT_e$, T_i, T_e are the negative of parallel current density, the total pressure, the parallel electron velocity, the ion pressure, the electron pressure, the ion temperature, and the electron temperature, respectively. They are divided into an equilibrium part and a perturbed part $\psi = \psi_{\rm eq} + \tilde{\psi}/\tilde{a}$, $\phi = \tilde{\phi}/\tilde{a}$, $n = n_{\rm eq} + \tilde{n}/\tilde{a}$, $T_i = T_{\rm eq} + \tilde{T}_i/\tilde{a}$, $T_e = \tau T_{\rm eq}$, $p_i = n_{\rm eq}T_{\rm eq} + T_{\rm eq}\tilde{n}/\tilde{a} + n_{\rm eq}\tilde{T}_i/\tilde{a}$, $p_e = \tau n_{\rm eq}T_{\rm eq} + \tau T_{\rm eq}\tilde{n}/\tilde{a}$. The electron temperature consists of a given equilibrium part $T_e = T_{\rm eq}$. The normalizations are $(tv_{ti}/a, r/\rho_i, \rho_i\nabla_\perp, a\nabla_\parallel, e\phi/T_0, \psi/\beta B_0\rho_i, n/n_0, T/T_0, v_\parallel/v_{ti}) \to (t, r, \nabla_\perp, \nabla_\parallel, \phi, \psi, n, T, v_\parallel)$.

The five-field mode for torus plasmas is able to describe the toroidal ion-temperature-gradient mode, KBM, IC, TM, and internal kink mode (table 2). Figure 1 shows the linear growth rate of drift-wave instabilities for a profile described in [77]. The ITG mode is unstable at low β and KBM (drift-resistive ballooning mode) appears at high β [8, 77]. The five-field model can be reduced by decreasing the number of fields. It is also reduced by applying for cylinder and slab plasmas. The reduction of geometry from a torus to cylinder is made by letting the inverse aspect ratio approach to zero $a/R_0 = 0$. When the geometry is simplified from a torus to a cylinder/slab, then toroidal ITG mode becomes a slab ITG (sITG) mode and the KBM becomes an electromagnetic IC, furthermore, the GAM is lost. This five-field model in a slab geometry is used in [29]. The five-field model is reduced to the standard four field model solving $(\phi, \psi, n, v_\parallel)$ [75] by omitting ion temperature fluctuation. The model is used to investigate interchange turbulence in a cylindrical plasma [24] and in a slab plasma [54]. In the cold ion limit, i.e. in the absence of ion diamagnetic velocity $\omega_{*i} = 0$, the four-field model is further reduced to a four field model that can describe the IC, TM, and drift-waves [78]. The four-field model is reduced to a three-field model solving (ϕ, ψ, n) by ignoring the parallel velocity. In this model the density can be replaced to the pressure by assuming a uniform temperature. The model is used to investigate the electromagnetic IC in a slab plasma [34, 35, 44]. The model can describe the IC and TM, and the drift-wave described in [79] is replaced to a simple drift-wave because of no parallel compressibility.

There is another way to reduce the model by considering a static magnetic island in the electrostatic limit. This model solves the five-field $(\phi, \psi, n, v_\parallel, T_i)$ and is used to investigate the electrostatic ITG turbulence in a static magnetic island in a slab plasma [50]. The model is further reduced to a three-field model by omitting ion temperature and parallel velocity (ϕ, ψ, n). This electrostatic model is used to investigate the influence of electrostatic interchange turbulence on a static magnetic island [28, 31]. These are summarized in table 2. It is remarked that there is a model including the electron temperature instead of the ion temperature in cylindrical plasmas [80].

2.2. Fluid model used in two-dimensional simulations

It this section we describe the five-field model in slab plasmas. A slab plasma corresponds to a radially localized region around a low (m, n) rational surface in a torus plasma as shown in figure 5. In two-dimensional slab plasmas the five-field equations become

$$\left(\frac{\partial}{\partial t} + \mathbf{v}\cdot\nabla\right)\nabla^2\phi = -\mathbf{B}\cdot\nabla J - d_i\beta\nabla\cdot(\mathbf{v}_{di}\cdot\nabla\nabla\phi) - K[p] + \mu\nabla^4\phi, \tag{6}$$

$$\left(\frac{\partial}{\partial t} + \mathbf{v}\cdot\nabla\right)n = -\mathbf{B}\cdot\nabla v_{e\parallel} + K[\phi - p_e] + \mu\nabla^2 n, \tag{7}$$

$$\left(\frac{\partial}{\partial t} + \mathbf{v}\cdot\nabla\right)v_\parallel = -\beta\mathbf{B}\cdot\nabla p + \mu\nabla^2 v_\parallel, \tag{8}$$

$$\frac{\partial\psi}{\partial t} = -\mathbf{B}\cdot\nabla\phi + d_i\beta\mathbf{B}\cdot\nabla p_e + \eta J, \tag{9}$$

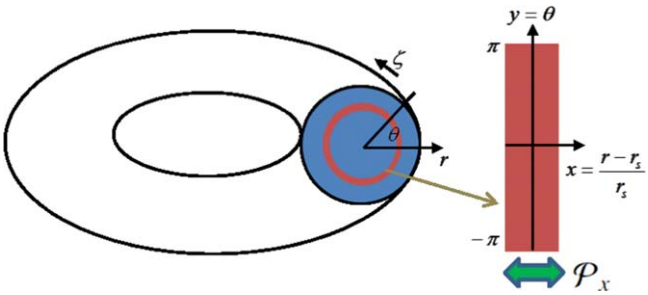

Figure 5. Parity operator $\mathcal{P}_x$ in the radial direction.

$$\left(\frac{\partial}{\partial t}+\mathbf{v}\cdot\nabla\right)T_i=-(\gamma-1)(\mathbf{B}\cdot\nabla v_{\parallel}+\kappa_L T_i)$$
$$+K[(\gamma-1)(\phi+T_i+n)+\gamma T_i]+\mu\nabla^2 T_i, \qquad (10)$$

where $\mathbf{v}\cdot\nabla f=[\phi,f]$, $\mathbf{B}\cdot\nabla f=-[\psi,f]$, $\mathbf{v}_{di}\cdot\nabla\nabla f=-[\nabla f,p_i]$, $K[f]=\kappa\frac{\partial f}{\partial y}$, are written in terms of the Poisson bracket $[f,g]=\mathbf{e}_z\cdot\nabla f\times\nabla g=\frac{\partial f}{\partial x}\frac{\partial g}{\partial y}-\frac{\partial g}{\partial x}\frac{\partial f}{\partial y}$, where $\nabla f=(\frac{\partial f}{\partial x},\frac{\partial f}{\partial y})$. In the equations $\mathbf{B}=B_0\mathbf{e}_z-\mathbf{e}_z\times\nabla\psi$, $\mathbf{v}=\mathbf{e}_z\times\nabla\phi$, $\mathbf{v}_{di}=\mathbf{e}_z\times\nabla p_i$ are the magnetic field, the $E\times B$ flow velocity, and the ion diamagnetic velocity, respectively. In slab plasmas, the parallel component is in the guide magnetic field direction along the z-axis. The normalizations are $(tv_A/L, x/L, \phi/(B_0v_AL), \psi/(B_0L), v_{\parallel}/v_A, n/n_0, T/T_0)\to(t, x, \phi, \psi, v_{\parallel}, n, T)$, where v_A is the Alfvén speed. The parameters $d_i=v_A/\Omega_i=\rho_i/\sqrt{\beta}$, η, β, $\gamma=5/3$, and L are the ion skin depth, the plasma resistivity, the plasma beta, the ratio of specific heats, and the system size, respectively, where Ω_i is the ion cyclotron frequency and ρ_i is the ion Larmor radius.

Magnetic field configuration on the (x, y) plane is a Harris current sheet, $\mathrm{d}\psi_{\mathrm{eq}}(x)/\mathrm{d}x=\tanh(x/L_s)$. The magnetic shear length L_s of the Harris sheet is associated with the gradient of current density. Since the slab plasma describes a radially localized region around a rational surface, this local parameter L_s controls the growth rate of tearing instability which is a spontaneous magnetic reconnection. When the current sheet is thin, i.e. L_s is small, the growth rate of TM is large. In the conventional MHD theory the stability parameter of TM $\Delta'=\frac{L_s}{2}[\mathrm{d}\ln\hat{\psi}/\mathrm{d}x]_{0-}^{0+}$ is obtained by solving the linearized form of $\mathbf{B}\cdot\nabla J=\mathbf{B}\cdot\nabla\nabla^2\psi=0$. An equilibrium is stable (unstable) to tearing instabilities when Δ' is negative (positive). The turbulence is driven by an ion temperature gradient represented by the parameter $\eta_i=L_n/L_T$, which is the ratio of density-gradient length $L_n=-(\mathrm{d}\ln n_{\mathrm{eq}}/\mathrm{d}x)^{-1}$ and ITG length $L_T=-(\mathrm{d}\ln T_{\mathrm{eq}}/\mathrm{d}x)^{-1}$. Both density and temperature gradients are assumed to be uniform, and L_n is the same as the system size $L_n=L$ in our simulations.

3. Parity

We discuss the parity of fluctuations in magnetized plasmas, and consider two parity symmetries. One is the parity that reflects the symmetry in the radial direction x in slab plasmas (figure 5) [26, 54]. The other is the parity that reflects the symmetry along the magnetic field line (figure 6) [7]. First, we describe the parity in the radial direction, then we explain the parity along the magnetic field line.

Figure 6. Parity operator $\mathcal{P}$ along the magnetic field line.

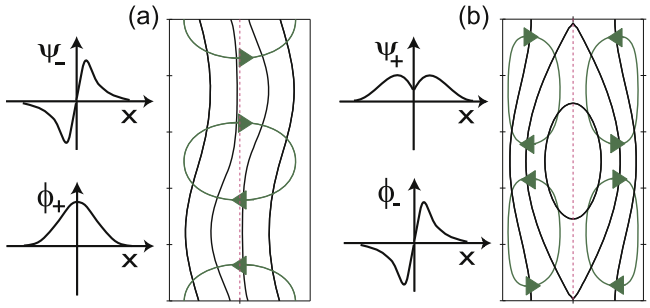

Figure 7. Electrostatic potential ϕ and perturbed magnetic flux ψ profiles of (a) twisting parity mode (ϕ_+, ψ_-) and (b) tearing parity mode (ϕ_-, ψ_+) in a slab plasma.

3.1. Parity symmetry in radial direction

We discuss the parity symmetry in radial direction near a rational surface. It is an extension from the parity of two-field model (reduced MHD) [26, 54] to the five-field model. Figure 7 illustrates the electrostatic potential ϕ and the perturbed magnetic flux ψ of twisting and tearing parity modes [54]. The mode is referred to as twisting parity mode, when ϕ (ψ) is even (odd) function of $x=r-r_s$, so that the $E\times B$ flow twists the magnetic surfaces, and the topology of the field lines does not change (figure 7(a)). On the other hand, the tearing parity mode exhibits the $E\times B$ flow which directs into the X-point, and the equi-contours of $\psi_{\mathrm{eq}}+\hat{\psi}\cos k_y y$ represent a magnetic island (figure 7(b)). We introduce the parity operator, whose rule of operation is to reflect $x\to -x$,

$$\mathcal{P}_x f(x, y, t)=f(-x, y, t). \qquad (11)$$

We rewrite the five-field equations equations (6)–(10) in terms of the Poisson bracket as

$$\frac{\partial\nabla^2\phi}{\partial t}+[\phi,\nabla^2\phi]=[\psi,\nabla^2\psi]-d_i\beta\nabla\cdot[\nabla\phi,p_i]$$
$$-K[p]+\mu\nabla^4\phi, \qquad (12)$$

$$\frac{\partial n}{\partial t}+[\phi,n]=[\psi,v_{\parallel}+d_i\nabla^2\psi]+K[\phi-p_e]+\mu\nabla^2 n, \qquad (13)$$

$$\frac{\partial v_{\parallel}}{\partial t}+[\phi,v_{\parallel}]=\beta[\psi,p]+\mu\nabla^2 v_{\parallel}, \qquad (14)$$

$$\frac{\partial \psi}{\partial t} + [\phi, \psi] = -d_i \beta [\psi, p_e] + \eta \nabla^2 \psi, \tag{15}$$

$$\frac{\partial T_i}{\partial t} + [\phi, T_i] = (\gamma - 1)(-[\psi, v_\parallel] + \kappa_L T_i) + K[(\gamma - 1)(\phi + T_i + n) + \gamma T_i] + \mu \nabla^2 T_i, \tag{16}$$

where $K[f] = 2\epsilon[x, f]$, $p = p_i + p_e$, $p_i = nT_i$, $p_e = nT_e$, and $T_e = T_{e0}$.

First, we consider the parity of perturbation governed by the linearized equations. We divide the field quantities into an equilibrium part and a perturbed part $f(x, y, t) = f_0(x) + \hat{f}(x, y, t)$. When the perturbation is sufficiently small $\hat{f} \ll f_0$, the equations can be linearized. We assume the equilibrium parts have a symmetry/asymmetry as $\mathcal{P}_x \psi_0(x) = \psi_0(x)$, $\mathcal{P}_x n_0(x) = -n_0(x)$, $\mathcal{P}_x T_{i0}(x) = -T_{i0}(x)$, $\phi_0 = v_{\parallel 0} = 0$, which are normally used in the analysis of interactions between turbulence and magnetic islands. Applying $\frac{1}{2}(1 \pm \mathcal{P}_x)$ to the linearized equations gives

$$\frac{\partial \nabla^2 \hat{\phi}_\pm}{\partial t} = [\psi_0, \nabla^2 \hat{\psi}_\mp] + [\hat{\psi}_\mp, \nabla^2 \psi_0] - d_i \beta \nabla \cdot [\nabla \hat{\phi}_\pm, p_{i0}] - K[p_\pm] + \mu \nabla^4 \hat{\phi}_\pm, \tag{17}$$

$$\frac{\partial \hat{n}_\pm}{\partial t} + [\hat{\phi}_\pm, n_0] = [\psi_0, \hat{v}_{\parallel \mp} + d_i \nabla^2 \hat{\psi}_\mp] + [\hat{\psi}_\mp, d_i \nabla^2 \psi_0] + K[\phi_\pm - p_{e\pm}] + \mu \nabla^2 \hat{n}_\pm, \tag{18}$$

$$\frac{\partial \hat{v}_{\parallel \mp}}{\partial t} = \beta[\hat{\psi}_\mp, p_0] + \beta[\psi_0, \hat{p}_\pm] + \mu \nabla^2 \hat{v}_{\parallel \mp}, \tag{19}$$

$$\frac{\partial \hat{\psi}_\mp}{\partial t} + [\hat{\phi}_\pm, \psi_0] = -d_i \beta [\psi_0, \hat{p}_{e\pm}] - d_i \beta [\hat{\psi}_\mp, p_{e0}] + \eta \nabla^2 \hat{\psi}_\mp, \tag{20}$$

$$\frac{\partial \hat{T}_{i\pm}}{\partial t} + [\hat{\phi}_\pm, T_{i0}] = (\gamma - 1)(-[\psi_0, \hat{v}_{\parallel \mp}] + \kappa_L \hat{T}_{i\pm}) + K[(\gamma - 1)(\phi_\pm + T_{i\pm} + n_\pm) + \gamma T_{i\pm}] + \mu \nabla^2 \hat{T}_{i\pm}, \tag{21}$$

where

$$f_\pm = \frac{1}{2}(1 \pm \mathcal{P}_x) f. \tag{22}$$

A set of $(\phi_+, \psi_-, n_+, v_{\parallel -}, T_{i+})$ is referred to as the twisting parity mode, and a set of $(\phi_-, \psi_+, n_-, v_{\parallel +}, T_{i-})$ is referred to as the tearing parity mode (table 4). Both of twisting and tearing parities are conserved during the linear growth, because they satisfy the linearized equations, respectively.

Next, we consider the parity symmetry of the nonlinear equations (12)–(16). We apply the parity operator $\mathcal{P}_x$ to equations (12)–(16), and by using $\mathcal{P}_x[f, g] = -[\mathcal{P}_x f, \mathcal{P}_x g]$, we have

$$\frac{\partial \nabla^2(-\mathcal{P}_x \phi)}{\partial t} + [-\mathcal{P}_x \phi, \nabla^2(-\mathcal{P}_x \phi)] = [\mathcal{P}_x \psi, \nabla^2 \mathcal{P}_x \psi] - d_i \beta \nabla \cdot [\nabla(-\mathcal{P}_x \phi), -\mathcal{P}_x p_i] - K[-\mathcal{P}_x p] + \mu \nabla^4(-\mathcal{P}_x \phi), \tag{23}$$

Table 4. Parities of perturbations in slab plasmas, where $\mathcal{P}_x f_\pm = \lambda_\pm f_\pm$ and $\lambda_\pm = \pm 1$.

Twisting parity	ϕ_+	ψ_-or $A_{\parallel -}$	n_+	$v_{\parallel -}$	T_+ or p_+
Tearing parity	ϕ_-	ψ_+ or $A_{\parallel +}$	n_-	$v_{\parallel +}$	T_- or p_-

$$\frac{\partial(-\mathcal{P}_x n)}{\partial t} + [-\mathcal{P}_x \phi, -\mathcal{P}_x n] = [\mathcal{P}_x \psi, \mathcal{P}_x v_\parallel + d_i \nabla^2 \mathcal{P}_x \psi] + K[-\mathcal{P}_x \phi - (-\mathcal{P}_x p_e)] + \mu \nabla^2(-\mathcal{P}_x n), \tag{24}$$

$$\frac{\partial \mathcal{P}_x v_\parallel}{\partial t} + [-\mathcal{P}_x \phi, \mathcal{P}_x v_\parallel] = \beta[\mathcal{P}_x \psi, -\mathcal{P}_x p] + \mu \nabla^2 \mathcal{P}_x v_\parallel, \tag{25}$$

$$\frac{\partial \mathcal{P}_x \psi}{\partial t} + [-\mathcal{P}_x \phi, \mathcal{P}_x \psi] = -d_i \beta [\mathcal{P}_x \psi, -\mathcal{P}_x p_e] + \eta \nabla^2 \mathcal{P}_x \psi, \tag{26}$$

$$\frac{\partial(-\mathcal{P}_x T_i)}{\partial t} + [-\mathcal{P}_x \phi, -\mathcal{P}_x T_i] = (\gamma - 1)(-[\mathcal{P}_x \psi, \mathcal{P}_x v_\parallel] + \kappa_L(-\mathcal{P}_x T_i)) + \mu \nabla^2(-\mathcal{P}_x T_i) + K[(\gamma - 1)(-\mathcal{P}_x \phi - \mathcal{P}_x T_i - \mathcal{P}_x n) + \gamma(-\mathcal{P}_x T_i)]. \tag{27}$$

These equations imply that when $(\phi, \psi, n, v_\parallel, T_i)$ satisfy the five-field equations, then $(-\mathcal{P}_x \phi, \mathcal{P}_x \psi, -\mathcal{P}_x n, \mathcal{P}_x v_\parallel, -\mathcal{P}_x T_i)$ satisfy the same equations. Hence, the tearing parity modes $(-\mathcal{P}_x \phi_-, \mathcal{P}_x \psi_+, -\mathcal{P}_x n_-, \mathcal{P}_x v_{\parallel +}, -\mathcal{P}_x T_{i-}) = (\phi_-, \psi_+, n_-, v_{\parallel +}, T_{i-})$ satisfy the nonlinear equations, and can remain tearing parity for all time, and thus the tearing parity mode is able to get saturated in its nonlinear evolution. On the other hand, $(\phi, \psi, n, v_\parallel, T_i)$ and $(\mathcal{P}_x \phi, -\mathcal{P}_x \psi, \mathcal{P}_x n, -\mathcal{P}_x v_\parallel, \mathcal{P}_x T_i)$ do not satisfy the same equations. Thus, the pure twisting parity mode does not satisfy the nonlinear equations, and therefor the twisting parity mode produces tearing parity modes through nonlinear terms in the nonlinear evolution. That is referred to as the nonlinear parity mixing.

3.2. Parity symmetry along a magnetic field line

Here, we consider the parity of ballooning type perturbations. This parity is discussed in local gyrokinetic simulations recently [7, 81], so we discuss the parity of gyrokinetic equations, which is used in the studies on interactions between turbulence and magnetic islands [55, 57–63]. We divide the distribution function into the Maxwellian part and a perturbed part $f_a = F_{Ma} + \hat{f}_a$ where $F_{Ma} = \frac{n_0}{(2\pi T_a / m_a)^{3/2}} \exp\left(-\frac{m_a v_\parallel^2}{2T_a} - \frac{\mu B}{T_a}\right)$ and a denotes particle species. The perturbation is expressed as $\hat{f}_a(\mathbf{X}, v_\parallel, \mu, t) = \sum_{\mathbf{k}_\perp} \hat{f}_{a\mathbf{k}_\perp}(k_x, k_y, z, v_\parallel, \mu, t) \exp(\mathrm{i} S_{\mathbf{k}_\perp})$, where $\nabla S_{\mathbf{k}_\perp} = \mathbf{k}_\perp$. The non-adiabatic part of the perturbed distribution function

$\hat{h}_{a\mathbf{k}_\perp} = \hat{f}_{a\mathbf{k}_\perp} + F_{Ma}\frac{q_a}{T_a}\hat{\phi}_{\mathbf{k}_\perp}J_{0a}$ obeys the gyrokinetic equation

$$\frac{\partial \hat{h}_{a\mathbf{k}_\perp}}{\partial t} = -\mathrm{i}\mathbf{v}_{da}\cdot\mathbf{k}_\perp\hat{h}_{a\mathbf{k}_\perp} - v_{Ta}[H,\,\hat{h}_{a\mathbf{k}_\perp}]_\parallel + q_a\frac{F_{Ma}}{T_a}\frac{\partial\hat{\chi}_{a\mathbf{k}_\perp}}{\partial t} + \mathrm{i}\mathbf{v}_{*a}\cdot\mathbf{k}_\perp q_a\frac{F_{Ma}}{T_a}\hat{\chi}_{a\mathbf{k}_\perp} + [\hat{\chi}_a,\,\hat{h}_a]_{\mathbf{k}_\perp} + C_a(\hat{h}_{a\mathbf{k}_\perp}), \tag{28}$$

where $\hat{\chi}_{a\mathbf{k}_\perp} = (\hat{\phi}_{\mathbf{k}_\perp} - v_{Ta}v_\parallel\hat{A}_{\parallel\mathbf{k}_\perp})J_{0a}$, $\mathbf{v}_{da}$, $\mathbf{v}_{*a}$, C_a, $v_\parallel$, μ, $v_{Ta} = \sqrt{T_a/m_a}$ are the generalized potential, the magnetic drift velocity, the diamagnetic drift velocity, the collision operator, the parallel velocity, the magnetic moment, and the thermal velocity, respectively. The operators are $[f,\,g]_{\mathbf{k}_\perp} \equiv \sum_{k'_\perp,k''_\perp}\delta_{\mathbf{k}_\perp,k'_\perp+k''_\perp}\mathbf{b}\cdot k'_\perp\times k''_\perp f_{k'_\perp}g_{k''_\perp}$, $[H,\,\hat{h}_{a\mathbf{k}_\perp}]_\parallel \equiv \nabla_\parallel H\frac{\partial\hat{h}_{a\mathbf{k}_\perp}}{\partial v_\parallel} - \frac{\partial H}{\partial v_\parallel}\nabla_\parallel\hat{h}_{a\mathbf{k}_\perp} = v_\parallel\nabla_\parallel\hat{h}_{a\mathbf{k}_\perp} - \mu\nabla_\parallel B\frac{\partial\hat{h}_{a\mathbf{k}_\perp}}{\partial v_\parallel}$, $\nabla_\parallel = \mathbf{b}\cdot\nabla$, where $H = v_\parallel^2/2 + \mu B$, and $J_{0a} = J_0(\rho_a k_\perp)$ is the 0th order Bessel function. We use magnetic flux coordinates, the magnetic flux label s, the poloidal angle θ, and the toroidal angle ζ, and the perpendicular wavenumber can be written as $\mathbf{k}_\perp = k_s\nabla s + k_\alpha\nabla(\zeta - q(s)\theta)$, where $\alpha = \zeta - q(s)\theta$ is the magnetic field line label. We omit the parallel component of magnetic perturbation for simplicity. The Poisson equation and Ampere's law are

$$\lambda_{Di}^2k_\perp^2\hat{\phi}_{\mathbf{k}_\perp} = \sum_a q_a\left(\int\hat{h}_{a\mathbf{k}_\perp}J_{0a}\mathrm{d}^3v - \frac{q_a}{T_a}\hat{\phi}_{\mathbf{k}_\perp}\right), \tag{29}$$

$$k_\perp^2\hat{A}_{\parallel\mathbf{k}_\perp} = \frac{\beta_i}{2}\sum_a q_a v_{Ta}\int v_\parallel\hat{h}_{a\mathbf{k}_\perp}J_{0a}\mathrm{d}^3v. \tag{30}$$

The normalizations are $(tv_{Ti}/R_0,\ \mathbf{k}_\perp\rho_{Ti},\ v_\parallel/v_{Ta},\ F_{Ma}v_{Ta}^3/n_0,\ \hat{f}_aR_0v_{Ta}^3/(\rho_{Ti}n_0),\ \hat{\phi}eR_0/(\rho_{Ti}T_i),\ \hat{A}_\parallel R_0/(\rho_{Ti}^2B_0),\ m_a/m_i,\ T_a/T_i,\ n/n_0,\ B/B_0,\ q_a/e,\ \lambda_{Di}/\rho_{Ti}) \to (t,\ \mathbf{k}_\perp,\ v_{\parallel a},\ F_{Ma},\ \hat{f}_a,\ \hat{\phi},\ \hat{A}_\parallel,\ M_a,\ T_a,\ n,\ B,\ q_a,\ \lambda_{Di})$, where $\lambda_{Di} = \sqrt{T_i/(4\pi e^2n_0)}$ and β_i is the normalized ion pressure. We rewrite coordinates $(s,\,\alpha,\,\theta) \to (x,\,y,\,z)$, so that $\mathbf{k}_\perp = (k_s,\,k_\alpha) \to (k_x,\,k_y)$. The parity operator is defined by using this coordinate

$$\mathcal{P}\hat{Q}(k_x,\,k_y,\,z,\,v_\parallel,\,\mu,\,t) = \hat{Q}(-k_x,\,k_y,\,-z,\,-v_\parallel,\,\mu,\,t). \tag{31}$$

We assume that the equilibrium magnetic field strength $B = |\mathbf{B}|$ is invariant under this transformation $\mathcal{P}B = B$ and there is no $E\times B$ flow shear.

We will show that when the perturbed gyro-center distribution function $\hat{f}_{a\mathbf{k}_\perp}(z,\,v_\parallel,\,\mu,\,t)$, the perturbed electrostatic potential $\hat{\phi}_{\mathbf{k}_\perp}(z,\,t)$, and the perturbed vector potential $\hat{A}_{\mathbf{k}_\perp}(z,\,t)$ satisfy equations (28)–(30) then $(-\mathcal{P}\hat{f}_{a\mathbf{k}_\perp},\,-\mathcal{P}\hat{\phi}_{\mathbf{k}_\perp},\,\mathcal{P}\hat{A}_{\parallel\mathbf{k}_\perp})$ also satisfy equations (28)–(30). In addition, $(\mathcal{P}\hat{f}_{a\mathbf{k}_\perp},\,\mathcal{P}\hat{\phi}_{\mathbf{k}_\perp},\,-\mathcal{P}\hat{A}_{\parallel\mathbf{k}_\perp})$ also satisfy the equations when the equations are linearized, so that both of tearing and twisting parities are conserved in the linear growth of instabilities. Each part in the equation is transformed as $\mathcal{P}\nabla_\parallel = -\nabla_\parallel$, $\mathcal{P}k_\perp = k_\perp$, $\mathcal{P}\mathbf{v}_{da}\cdot\mathbf{k}_\perp = \mathbf{v}_{da}\cdot\mathbf{k}_\perp$, $\mathcal{P}\mathbf{v}_{*a}\cdot\mathbf{k}_\perp = \mathbf{v}_{*a}\cdot\mathbf{k}_\perp$, $\mathcal{P}F_{Ma}(z,\,v_\parallel,\,\mu) = F_{Ma}(z,\,v_\parallel,\,\mu)$. These are easily confirmed, for instance, for large aspect ratio tokamaks $\mathbf{v}_{*a}\cdot\mathbf{k}_\perp = k_y\frac{-T_a}{q_aL_nB}[1 + (\frac{v_\parallel^2}{2} + \mu B - \frac{3}{2})\eta_a]$, $\mathbf{v}_{da}\cdot\mathbf{k}_\perp = \frac{-T_a}{q_aRB}(v_\parallel^2 + \mu B)(k_x\sin z + k_y(\cos z + \hat{s}z\sin z))$, $k_\perp^2 = k_y^2[1 + \hat{s}^2(\theta - \theta_k)^2] = (k_x + \hat{s}zk_y)^2 + k_y^2$, where $\theta_k = -k_x/(k_y\hat{s})$.

Table 5. Parities of perturbations, where $\mathcal{P}\hat{f}^\pm = \lambda_p^\pm\hat{f}^\pm$ and $\lambda_p^\pm = \pm1$.

Twisting parity	$\hat{f}^+_{s\mathbf{k}_\perp}$,	$\hat{\phi}^+_{\mathbf{k}_\perp}$,	$\hat{A}^-_{\parallel\mathbf{k}_\perp}$,	$\hat{\chi}^+_{s\mathbf{k}_\perp}$,	$\hat{h}^+_{s\mathbf{k}_\perp}$
Tearing parity	$\hat{f}^-_{s\mathbf{k}_\perp}$,	$\hat{\phi}^-_{\mathbf{k}_\perp}$,	$\hat{A}^+_{\parallel\mathbf{k}_\perp}$,	$\hat{\chi}^-_{s\mathbf{k}_\perp}$,	$\hat{h}^-_{s\mathbf{k}_\perp}$

By applying the operator $\mathcal{P}$ to the Poisson equation and Ampere's law, equations (29) and (30), we have

$$\lambda_{Di}^2k_\perp^2\mathcal{P}\hat{\phi}_{\mathbf{k}_\perp} = \sum_a q_a\left(\int\mathcal{P}\hat{h}_{a\mathbf{k}_\perp}J_{0s}\mathrm{d}^3v - \frac{q_a}{T_a}\mathcal{P}\hat{\phi}_{\mathbf{k}_\perp}\right), \tag{32}$$

$$k_\perp^2\mathcal{P}\hat{A}_{\parallel\mathbf{k}_\perp} = \frac{\beta_i}{2}\sum_a q_a v_{Ta}\int v_\parallel(-\mathcal{P}\hat{h}_{a\mathbf{k}_\perp}J_{0s})d^3v. \tag{33}$$

These imply that the electrostatic potential $\hat{\phi}_{\mathbf{k}_\perp}$ has the same parity as the perturbed distribution function $\hat{f}_{a\mathbf{k}_\perp}$, while the vector potential $\hat{A}_{\parallel\mathbf{k}_\perp}$ has the opposite parity, and thus the generalized potential $\hat{\chi}_{\mathbf{k}_\perp}$ has the same parity as $\hat{f}_{a\mathbf{k}_\perp}$ as summarized in table 5. Next, we apply the operator $\mathcal{P}$ to the gyrokinetic equation (28) and have

$$\frac{\partial(-\mathcal{P}\hat{h}_{a\mathbf{k}_\perp})}{\partial t} = -\mathrm{i}\mathbf{v}_{da}\cdot\mathbf{k}_\perp(-\mathcal{P}\hat{h}_{a\mathbf{k}_\perp}) - v_{Ta}[H,\,-\mathcal{P}\hat{h}_{a\mathbf{k}_\perp}]_\parallel + q_a\frac{F_{Ma}}{T_a}\frac{\partial(-\mathcal{P}\hat{\chi}_{a\mathbf{k}_\perp})}{\partial t} + \mathrm{i}\mathbf{v}_{*a}\cdot\mathbf{k}_\perp q_a\frac{F_{Ma}}{T_a}(-\mathcal{P}\hat{\chi}_{a\mathbf{k}_\perp}) + [-\mathcal{P}\hat{\chi}_a,\,-\mathcal{P}\hat{h}_a]_{\mathbf{k}_\perp} + C_a(-\mathcal{P}\hat{h}_{a\mathbf{k}_\perp}). \tag{34}$$

When $(\hat{f}_{a\mathbf{k}_\perp},\,\hat{\phi}_{\mathbf{k}_\perp},\,\hat{A}_{\parallel_{\mathbf{k}_\perp}})$ satisfy the nonlinear gyrokinetic equation, $(-\mathcal{P}\hat{f}_{a\mathbf{k}_\perp},\,-\mathcal{P}\hat{\phi}_{\mathbf{k}_\perp},\,\mathcal{P}\hat{A}_{\parallel_{\mathbf{k}_\perp}})$ also satisfy the same equation, and therefore tearing parity modes $(-\mathcal{P}\hat{f}^-_{a\mathbf{k}_\perp},\,-\mathcal{P}\hat{\phi}^-_{\mathbf{k}_\perp},\,\mathcal{P}\hat{A}^+_{\parallel_{\mathbf{k}_\perp}}) = (\hat{f}^-_{a\mathbf{k}_\perp},\,\hat{\phi}^-_{\mathbf{k}_\perp},\,\hat{A}^+_{\parallel_{\mathbf{k}_\perp}})$ satisfy the nonlinear gyrokinetic equation, where

$$\hat{f}^\pm_{a\mathbf{k}_\perp} = \frac{1}{2}(1\pm\mathcal{P})\hat{f}_{a\mathbf{k}_\perp}. \tag{35}$$

On the other hand, the twisting parity mode $(\mathcal{P}\hat{f}^+_{a\mathbf{k}_\perp},\,\mathcal{P}\hat{\phi}^+_{\mathbf{k}_\perp},\,-\mathcal{P}\hat{A}^-_{\parallel_{\mathbf{k}_\perp}}) = (\hat{f}^+_{a\mathbf{k}_\perp},\,\hat{\phi}^+_{\mathbf{k}_\perp},\,\hat{A}^-_{\parallel_{\mathbf{k}_\perp}})$ does not satisfy the nonlinear equation. However, when the gyrokinetic equation equation (28) is linearized, i.e. nonlinear term $[\hat{\chi}_a,\,\hat{h}_a]_{\mathbf{k}_\perp}$ is neglected, it is shown that the twisting parity mode also satisfies the equation by multiplying -1 to equation (34) and using equation (35). Hence, both the tearing and twisting parity modes satisfy the linearized equation, and the parity is conserved during the linear growth of instabilities. In other words, we can divide the perturbed distribution function into the twisting and tearing parity parts $\hat{f}_{a\mathbf{k}_\perp} = \hat{f}^+_{a\mathbf{k}_\perp} + \hat{f}^-_{a\mathbf{k}_\perp}$ and they are independent in the linear growth. For instance, the ITG mode, TEM, and KBM are the twisting parity mode, and their electrostatic potentials $\hat{\phi}^+_{\mathbf{k}_\perp}$ (vector potential $\hat{A}^-_{\parallel_{\mathbf{k}_\perp}}$) are the even (odd) function of z as shown in figures 4 and 5 in [7], while MTM is the tearing parity mode. When the amplitude of instability becomes finite and the nonlinearity plays a role, then the tearing parity mode can keep its parity. However, the twisting parity mode cannot keep its parity,

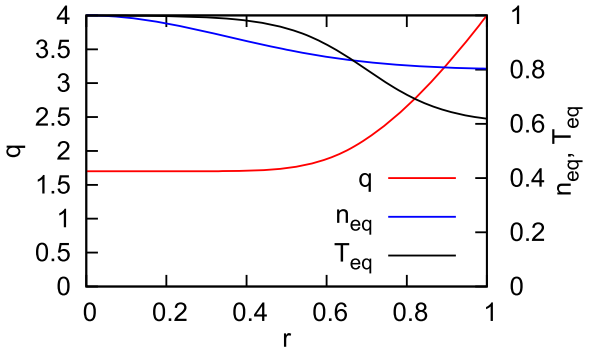

Figure 8. Initial equilibrium profiles.

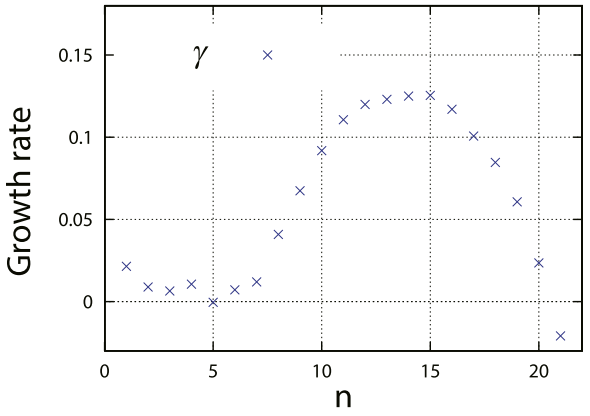

Figure 9. Linear growth rate as a function of toroidal mode number n for the initial equilibrium of the flux-driven simulation. The tearing mode is represented by $n = 1$ and the KBMs are $7 \leqslant n \leqslant 20$. Reproduced courtesy of IAEA. Figure from [30]. Copyright 2009 IAEA.

and the energy is transferred from the twisting parity mode to tearing parity modes. For instance, when the ITG mode gets saturated, the tearing parity modes must be produced, and the excitation of stable tearing parity modes influences the amplitude of ITG turbulence [81]. The nonlinear parity mixing is ubiquitous in drift-wave turbulence, and it also happens in nonlinear evolution of instabilities driven by energetic particles [82]. This nonlinear parity mixture is represented by the equations for tearing parity mode $\hat{h}^{-}_{a\mathbf{k}_\perp}$ and twisting parity mode $\hat{h}^{+}_{a\mathbf{k}_\perp}$ obtained by applying $\frac{1}{2}(1 \pm \mathcal{P})$ to the gyrokinetic equation equation (28)

$$\frac{\partial}{\partial t}\left(\hat{h}^{-}_{a\mathbf{k}_\perp} + q_a \frac{F_{Ma}}{T_a}\hat{\chi}^{-}_{a\mathbf{k}_\perp}\right) = [\hat{\chi}^{+}_a, \hat{h}^{+}_a]_{\mathbf{k}_\perp} + [\hat{\chi}^{-}_a, \hat{h}^{-}_a]_{\mathbf{k}_\perp}, \quad (36)$$

$$\frac{\partial}{\partial t}\left(\hat{h}^{+}_{a\mathbf{k}_\perp} + q_a \frac{F_{Ma}}{T_a}\hat{\chi}^{+}_{a\mathbf{k}_\perp}\right) = [\hat{\chi}^{+}_a, \hat{h}^{-}_a]_{\mathbf{k}_\perp} + [\hat{\chi}^{-}_a, \hat{h}^{+}_a]_{\mathbf{k}_\perp}, \quad (37)$$

where the linear terms are omitted because they conserve the parity. Equation (36) implies that tearing parity modes are produced by nonlinear interactions between the same parity modes, and thus the tearing parity mode satisfy the nonlinear gyrokinetic equation, because their nonlinear interactions are represented by $[\hat{\chi}^{-}_a, \hat{h}^{-}_a]_{\mathbf{k}_\perp}$. Equation (37) implies, on the other hand, that twisting parity modes are produced by nonlinear interactions between opposite parity modes, and equation (36) clearly

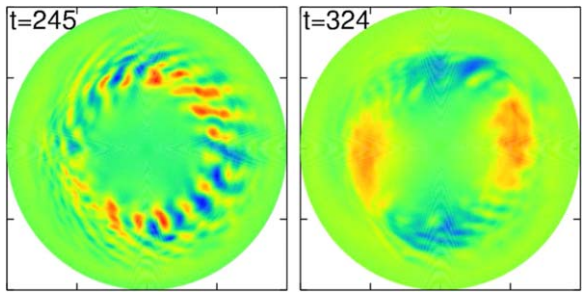

Figure 10. Color-map of electrostatic potential on a poloidal cross section. The quasi-equilibrium of micro-turbulence is formed at $t = 245$. The mixture of micro-turbulence and magnetic islands due to the tearing mode is established at $t = 324$. Reproduced courtesy of IAEA. Figure from [30]. Copyright 2009 IAEA.

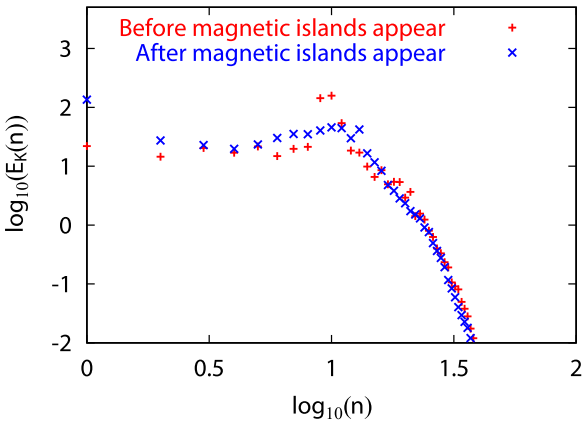

Figure 11. Toroidal mode number spectrum of $E \times B$ flow energy, where n is the toroidal mode number. Magnetic islands due to the tearing mode is denoted by $n = 1$, and the peak of KBMs is located at $n = 10$. The $n = 2 - 8$ modes are the coherent stable modes. Reproduced courtesy of IAEA. Figure from [30]. Copyright 2009 IAEA.

demonstrates that nonlinear interactions between twisting parity modes $[\hat{\chi}^{+}_a, \hat{h}^{+}_a]_{\mathbf{k}_\perp}$ produce tearing parity modes $(\hat{h}^{-}_{a\mathbf{k}_\perp}\hat{\chi}^{-}_{a\mathbf{k}_\perp})$.

4. Unstable against TM

In this section we present multi-scale interactions between turbulence and magnetic islands caused by the TM and their influence on turbulent transport by reviewing a flux-driven electromagnetic simulation [30] and by discussing each part of interactions in subsections.

4.1. Flux driven electromagnetic turbulence with TM

We review three-dimensional numerical simulations of flux-driven turbulent transport in a toroidal plasma controlled by external heat source and sink [30] as a typical multi-scale simulation of turbulence and magnetic islands. This is also a self-consistent calculation of the interactions between turbulence, zonal flows, GAM and magnetic islands by numerically

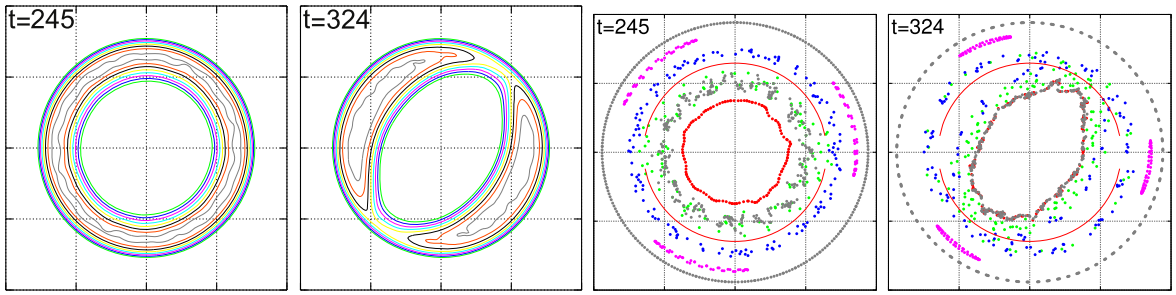

Figure 12. Equi-contours of helical flux function of $m/n = 2$ on a poloidal cross section (left two frames). Poincare map of magnetic field lines (right two frames), where red solid line indicates $q = 2$ rational surface. There is no magnetic islands at $t = 245$. Magnetic islands with $(m, n) = (2, 1)$ appear at $t = 324$. Reproduced courtesy of IAEA. Figure from [30]. Copyright 2009 IAEA.

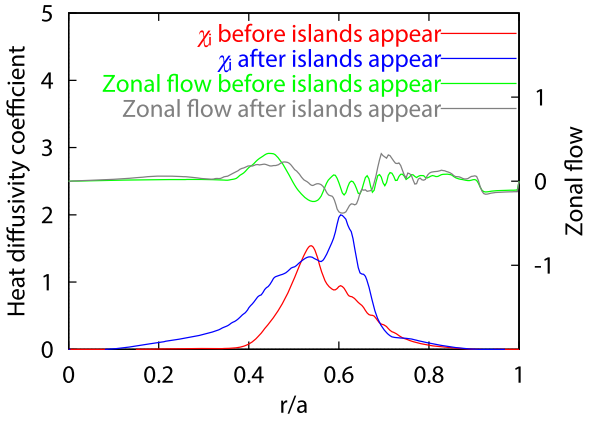

Figure 13. Profile of χ_i and zonal flows before and after the appearance of magnetic islands in flux-driven electromagnetic turbulence. The magnetic islands appear on $q(r_s) = 2$ rational surface at $r_s/a = 0.6$. Reproduced courtesy of IAEA. Figure from [30]. Copyright 2009 IAEA.

solving a reduced set of two-fluid equations (1)–(5). The flux-driven simulation enables us to investigate the influence of the temperature profile flattening inside the separatrix of island, which is controlled by a balance among the heat source, the turbulent transport and the violation of magnetic surfaces.

We consider a plasma which is unstable against a TM and KBMs [30]. We set $\epsilon = 0.25$, $\rho_i/a = 1/80$, $\tau \equiv T_e/T_i = 1$, $\beta = 0.01$, the artificial dissipation $\mu = m^4 10^{-7}$, and the normalized resistivity $\eta = 4 \times 10^{-4}$ which corresponds to the Lundquist number $S \equiv v_A a/\eta = 1.6 \times 10^6$. The q-profile is set to have a $q(r_s) = 2$ rational surface as shown in figure 8, so that an $(m, n) = (2, 1)$ TM can be unstable. The initial profile in figure 8 is unstable against KBM/drift-resistive ballooning mode and the TM (figure 9) [30]. Since the growth rate of the KBM is much larger than the TM, the KBM driven turbulent state is established at the beginning as shown in the color map of electrostatic potential profile in figure 10. We have zonal flows produced from the KBM, but the flows are not so strong that the streamer of the KBM remains. Note that the coherent $(m, n) = (2, 1)$ mode is excited and has a similar level as the other modes as shown in figure 11, however this mode is not a coherent $(m, n) = (2, 1)$ magnetic island but narrow magnetic islands with $W \ll a$ which is a part of turbulence as shown by contours of magnetic flux and Poincare map of magnetic field lines in figure 12 [25]. The details are discussed in the next section. This quasi-steady KBM turbulent state continues until the magnetic islands of TM appears.

After the magnetic islands of TM appear, violated magnetic surfaces form into the $(m, n) = (2, 1)$ islands shown in figure 12. Then, turbulent perturbations appearing at the bad curvature region are transformed to the perturbations reflecting the $(m, n) = (2, 1)$ magnetic island in the electrostatic potential profile in figure 10. The turbulence can be strong at the X-point because the gradient is kept [57], while it can be also strong around the O-point because the magnetic perturbation of the island reduces the magnetic shear at the O-point as suggested by the equation $\mathrm{d}B_y/\mathrm{d}x = B_0/L_s + \Psi'' \cos ky$ [32]. In this simulation there is little difference of turbulent fluctuation in the poloidal direction at $t = 324$ as shown in figure 10, and thus the difference of the turbulence intensity between the X and O points is small.

Although the KBM is suppressed by the appearance of the magnetic islands, the mutual interactions between turbulence and islands enhance heat transport as shown by the ion heat diffusivity profile in figure 13. The ion heat diffusivity $\chi_i = -Q_i/(\mathrm{d}\langle T_i\rangle/\mathrm{d}r)$ is calculated with respect to the unperturbed flux surfaces, i.e. it is averaged over the poloidal angle. We omit the parallel streaming along the magnetic field line and evaluate the heat flux by $Q_i = -\tilde{a}\langle \tilde{T}_i \nabla_\theta \tilde{\phi}\rangle$ in order to eliminate the transport due to the magnetic perturbation of the island. The diffusivity χ_i increases at $r/a = 0.6$, where the magnetic islands appear. The enhancement of χ_i takes place at the inside of the separatrix of the island, while the diffusivity is a little decreased just outside of the separatrix of the island, which is located at $r/a = 0.55$ and 0.7. The enhancement of diffusivity is mainly attributed to the appearance of coherent mode described in detail in the next subsection.

As a results of the multi-scale interactions, χ_i is enhanced inside the separatrix of the magnetic islands, however, the ion temperature profile is not completely flattened inside the island as shown by the profile of ion temperature gradient $-\mathrm{d}T_i/\mathrm{d}r$ in figure 14 [30], in addition, the profile is steepened just outside of the island. It is noted that the profile is averaged over the poloidal angle, and thus the flattening and steepening of the profile results from the average over the O and X points. When a magnetic island appears in the absence of turbulence, we expect that the profile is steepened outside and flattened inside the island around the O-point, and the

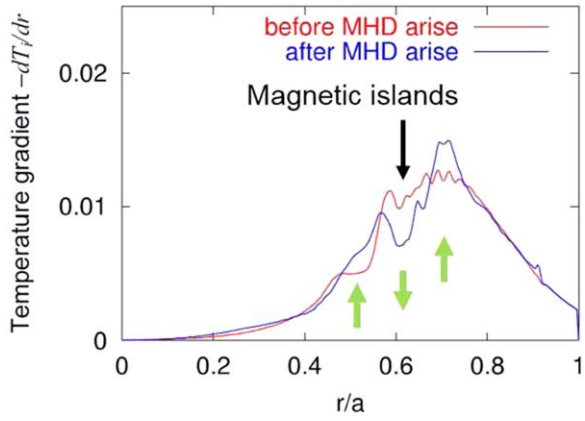

Figure 14. Ion temperature gradient profile $-\mathrm{d}T_i/\mathrm{d}r$ before and after the appearance of magnetic islands (MHD) in flux-driven electromagnetic turbulence. The magnetic islands appear at $r/a = 0.6$.

profile is steepened around the X-point. The interaction between turbulence and magnetic island causes deviation from these profiles around the island. The turbulent fluctuations mix the difference of temperature at the O and X points, and result in the flattening inside and steepening outside the island. The incomplete ion temperature profile flattening inside the island and the steepening at outside are consistent with the experimental observation of the ion temperature profile around magnetic islands interacting with turbulence in DIII-D plasmas [69]. In addition [69], reports increased fluxes when the gradients are decreased inside the island. This implies that the power balance effective radial diffusivities are increased at the rational surface of the island, and it is also consistent with the increase of thermal diffusion χ_i profile in figure 13. This incomplete flattening is also observed in non-flux-driven simulations of interactions between turbulence and magnetic islands [44–46, 55, 57]. Gyrokinetic simulations show that the ion temperature is not completely flattened by electrostatic toroidal ITG turbulence [55, 57]. Similar incomplete flattening of pressure profile is also observed as a results of interactions between a magnetic island and the resistive MHD interchange turbulence in slab plasmas [44]. Other fluid simulations also demonstrate that the electrostatic ITG turbulence is also able to maintain finite temperature gradient across the magnetic island [45, 46].

4.2. Coherent vortex flows

The violation of ballooning structure of turbulence is observed in figure 10, and is also shown by the toroidal wavenumber spectrum of $E \times B$ flow energy in figure 11 [30]. The peak of KBM occurs at $n = 10$ in the quasi-steady turbulent state, which is dominated by ballooning like turbulent fluctuations. Then, after the magnetic islands due to the TM appear, the peak at $n = 10$ disappears and the spectrum is broadened, so that the large-scale stable modes with $1 < n < 8$ are excited resulting in coherent/meso-scale vortex flow [30]. The excitation of coherent vortex flow by the multi-scale interactions is clearly shown in [29], which made comparison between the energy spectra of turbulence alone, TM alone, and mixture of turbulence and TM. The energy spectrum of the mixture of turbulence and TM has higher amplitude at low wavenumber than that of TM alone. This coherent vortex formation is generally observed in interactions between turbulence and magnetic islands: five-field fluid simulations of KBM [8, 25], three-field fluid simulations of resistive MHD IC in slab plasmas [39] and gyrokinetic simulations of ITG turbulence [55, 57, 59].

Here we consider the energy transfer to coherent vortex flow such as the $(m, n) = (2, 1)$ mode. The energy transfer from the KBM turbulence to the coherent modes is evaluated [30], and the energy transfer from resistive MHD IC to the coherent mode is investigated [34]. The equation of the (m, n) flow energy is obtained from the (m, n) Fourier component of the vorticity equation equation (1) as

$$\frac{\mathrm{d}}{\mathrm{d}t}\int \frac{1}{2}V_{E\times\, Bmn}^2 \mathrm{d}^3x = T_{\mathrm{R}mn} + T_{\mathrm{M}mn} + T_{\mathrm{LB}mn} + T_{\mathrm{KI}mn} + T_{\mathrm{ID}mn} + T_{\mathrm{LID}mn} + T_{\mathrm{C}mn}, \tag{38}$$

where

$$T_{\mathrm{R}mn} = \int \phi_{mn}\tilde{a}([\phi, \nabla_\perp^2\phi])_{mn}\mathrm{d}^3x,$$

$$T_{\mathrm{M}mn} = \int \phi_{mn}\frac{1}{n_{\mathrm{eq}}}(\nabla_\parallel J)_{mn}\mathrm{d}^3x,$$

$$T_{\mathrm{ID}mn} = \int \phi_{mn}\frac{\tilde{a}}{n_{\mathrm{eq}}}(\nabla_\perp\cdot[\nabla_\perp\phi, p_i])_{mn}\mathrm{d}^3x,$$

$$T_{\mathrm{C}mn} = \int \phi_{mn}\frac{1}{n_{\mathrm{eq}}}(K[p])_{mn}\mathrm{d}^3x,$$

$$T_{\mathrm{LB}mn} = \int \phi_{mn}\frac{1}{n_{\mathrm{eq}}}(\nabla_\parallel)_{\mathrm{eq}}J_{mn}\mathrm{d}^3x,$$

$$T_{\mathrm{KI}mn} = \int \phi_{mn}\frac{1}{n_{\mathrm{eq}}}(\nabla_\parallel)_{mn}J_{\mathrm{eq}}\mathrm{d}^3x,$$

$$T_{\mathrm{LID}mn} = \int \phi_{mn}\frac{\tilde{a}}{n_{\mathrm{eq}}}(\nabla_\perp\cdot[\nabla_\perp\phi_{mn}, p_{i\mathrm{eq}}])\mathrm{d}^3x,$$

are contribution to the flow drive from the Reynolds stress, the Maxwell stress, the nonlinear ion diamagnetic term, the toroidal curvature term, the magnetic field line bending term, the kink term, and the linear ion diamagnetic term, respectively. In the equation $\mathbf{V}_{E\times Bmn} = \mathbf{b}\times\nabla\phi_{mn}$ is the $E\times B$ flow velocity of (m, n) mode, $(\nabla_\parallel)_{mn}f = -\beta\tilde{a}[\psi_{mn}, f]$, $(\nabla_\parallel)_{\mathrm{eq}}f = \epsilon\partial_\zeta f - \beta\tilde{a}[\psi_{\mathrm{eq}}, f]$, $f_{mn} = \hat{f}_{mn}\mathrm{e}^{\mathrm{i}m\theta-\mathrm{i}n\zeta} + \hat{f}_{-m-n}\mathrm{e}^{-\mathrm{i}m\theta+\mathrm{i}n\zeta}$, where $\hat{f}_{mn}$ is the (m, n) Fourier component of f. The ion diamagnetic term comes from the gyro-viscous cancellation of gyro-stress tensor[79, 83]. The line bending term $T_{\mathrm{LB}mn}$ has a stabilizing effect on MHD instabilities, and it is related to the propagation of Alfvén wave along equilibrium magnetic field line. The kink term has a destabilizing effect on current-driven MHD instabilities, such as tearing instability. By evaluating each term in equation (38) we found the energy transfer from turbulent fluctuations to coherent vortex flow such as $V_{E\times B21}$. The Reynolds stress drives the coherent vortex flow, while the Maxwell stress and ion diamagnetic term suppress the flow production [8]. Hence, the Maxwell stress counteracts with the Reynolds stress in producing coherent vortex flow related to the magnetic islands. That is similar to the energy transfer from

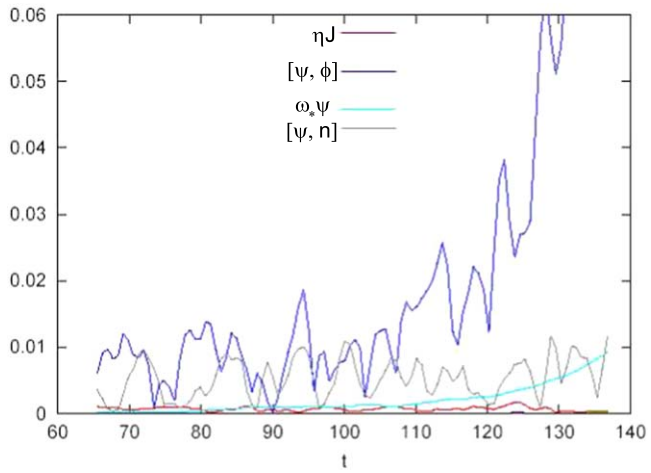

Figure 15. Time evolution of the absolute value of each term in the $(m, n) = (2, 1)$ component of Ohm's law on the $q = 2$ rational surface. The turbulent diffusion terms $[\hat{\psi}, \hat{\phi}]$ and $[\hat{\psi}, \hat{n}]$ (blue and gray lines) are significantly larger than the normal resistive diffusion term ηJ (red line).

turbulence to zonal flows $V_{E\times B00}$ that is driven by the Reynolds stress and suppressed by the Maxwell stress and ion diamagnetic term.

The coherent vortex flow can be caused not only by small-scale turbulence but by the stagnation of $E \times B$ flow to magnetic islands as expected by equation (4). This flow generation process is related to zonal flow modification by magnetic island and is discussed in the next subsection.

4.3. Zonal flows

Zonal flows play a role in the nonlinear interactions of drift-wave turbulence, although they are not strong in finite β plasmas, they regulate turbulence and also reduce the growth of islands by shearing the radial structures [84]. On the other hand, zonal flows are influenced not only by the turbulence but also by magnetic islands because the fluid flow tends to follow the reconnected magnetic surfaces, which is related to the polarization current.

The suppression of heat diffusivity just outside of the separatrix of magnetic island is consistent with the change of zonal flow profile in figure 13. The zonal flow profile is corrugated with meso-scale radial wavelength in the turbulent state before the islands appear in figure 13 [30]. After the appearance of magnetic islands, the flow profile is changed to have strong flow shear at the separatrix of the island, because the flow is stagnated around the O-point of the island. The zonal $E \times B$ flow modification is also observed in gyrokinetic simulations with stationary magnetic islands, and the shearing of flow modified by the island is strong enough to suppress TEMs [63]. The influence of the multi-scale interactions on the zonal flow is extensively investigated by using five-field model in a slab plasma [29, 40]. Interactions between electromagnetic sITG and TM cause oscillatory electromagnetic torque, and this torque causes oscillatory zonal flows that are different from GAM because it appears in slab plasmas. Since the zonal flows become oscillatory, the turbulent transport is not efficiently suppressed by the zonal flows [29]. As a back reaction to the magnetic island, the oscillatory zonal flows make magnetic islands oscillate, and that is called the magnetic island seesaw [40]. The oscillatory flow is also observed in gyrokinetic simulations [59].

4.4. Magnetic field stochasticity

The appearance of magnetic island at $q = 2$ rational surface is clearly shown by the equi-contours of $m/n = 2/1$ helical flux in figure 12 [30]. The equi-contours represent the magnetic surfaces when the magnetic perturbations have single helicity, which is $m/n = 2/1$ in this case, in cylindrical/slab plasmas. When magnetic perturbations have multi-helicity in torus plasmas, the Poincare map obtained by field line tracing is different from the equi-contours as shown in figure 12. It is remarked that points with same color are on a magnetic field line in the Poincare map in figure 12. Before the magnetic islands appear ($t = 245$), the Poincare map reflects the turbulent magnetic perturbation due to KBM. Then, after the growth of TM ($t = 324$), the $(m, n) = (2, 1)$ magnetic islands appear on the $q = 2$ rational surface represented by a red line. The field line orbit passing around the separatrix is unstable, as indicated by the blue points. Thus, the stochasticity of field line around the X-point is enhanced. This enhancement of the stochasticity around the X-point is also observed in gyrokinetic simulations [61].

4.5. Anomalous current drive

We have seen that coherent magnetic islands dominate turbulent fluctuations when TMs are unstable. However, when the islands are small, i.e. when the TM is growing, the turbulence can influence the growth of TM by anomalous current drive. Here we present the anomalous current drive due to the KBM turbulence. Figure 15 shows time evolution of the amplitude of each term on the $q = 2$ rational surface for the $(m, n) = (2, 1)$ mode of the generalized Ohm's law equation (4). The resistive diffusion term $\eta\nabla_\perp^2\tilde{\psi}$ is represented by the red line, and the anomalous turbulent drive terms, which are the nonlinear terms $[\tilde{\psi}, \tilde{\phi}]$ and $[\tilde{\psi}, \tilde{p}_e]$, are denoted by blue and gray lines, respectively. The nonlinear terms are significantly larger than the normal resistivity term, and thus the turbulence causes anomalous current drive. The anomalous current drive by sITG turbulence is also observed, and it is evaluated to be 10 or 100 times of the normal resistivity [50]. Nonlinear mixing of magnetic flux by $E \times B$ flow influence the magnetic island not only by enhancing growth rate but also by causing the oscillation of magnetic island, which is caused by small-scale dynamo-generated current and is referred to as magnetic island seesaw [40].

4.6. Non-flux-driven simulations

Most of the simulations of multi-scale interactions between turbulence and magnetic islands are non-flux-driven simulations as shown in table 2. Some of interactions between turbulence and magnetic islands are lost in non-flux-driven simulations, for instance, once the profile is completely

flattened inside of the separatrix of the islands, then the drive of turbulence is lost after the appearance of the islands. Thus, the non-flux-driven simulations do not capture an essential part of interactions between magnetic islands and turbulence driven by the temperature and density gradients. On the other hand, the initial process of magnetic island appearance in turbulent state is not sensitive to the profile flattening, and thus the non-flux-driven simulations well describe the process of the interactions, for instance, the energy transfer from small-scale turbulence to coherent modes is a general feature. This feature is observed not only for TMs but also for double TM in the quasi-steady equilibrium formed by a balance between micro-turbulence and zonal flow [25]. It is noted that the energy transfer to coherent modes does not mean the appearance of magnetic islands, because the mechanism of double TM appearance is a positive feedback loop between suppression of the zonal flow and growth of magnetic reconnection [25]. The difference of double TM from the TM is that the reduction of sheared flow caused by the turbulence between two island chains is needed to the appearance of islands. Thus, when the radial location of the peak of turbulence intensity is away from the radial location of the rational surface, where the island is expected to arise, zonal flows and the excitation of non-resonant modes between these two radial locations have significant impact on the interactions [25, 47].

5. Stable to TM

We have reviewed interactions between electromagnetic turbulence and magnetic islands, when TMs are unstable, and discussed the influence of the interactions on turbulent transport in the presence of magnetic islands in torus plasmas. Here, we consider the multi-scale interactions between turbulence and magnetic island, when TMs are stable. We will present that large-scale magnetic islands are influenced by small-scale turbulence, when the TM is stable/marginally stable, then we will discuss the parity mixture in the interactions.

This issue is linked to the excitation of NTMs [9, 74], which restrict the achievable β of tokamak plasmas. The NTM is nonlinearly destabilized by the perturbed bootstrap current in the presence of seed magnetic island, even when Δ' is negative. This seed magnetic island can be excited by turbulence [22]. It is demonstrated that the ITG turbulence can excite magnetic islands with widths equal to several times the ion Larmor radius $W \simeq 5\rho_i$, which is similar to the required seed island width [9] by fluid simulations in slab plasmas [37]. Then gyrokinetic simulations [61, 62], which include accurate finite Larmor radius effects, show that $W \simeq 3.6\rho_i$. Magnetic islands are also produced by an MHD IC for $\Delta' < 0$ in a slab plasma [37]. In addition, it is presented that islands are formed by an MHD IC with diamagnetic effects when the TM is marginally stable $\Delta' \simeq 0$ in slab plasmas [39] (table 1), and the pressure profile flattening inside the separatrix of the island is also investigated [52]. Such islands formation is also shown by ICs appearing the location away from the rational surface [47]. In addition, fluid simulations show the growth of NTMs seeded by the MHD-interchange-driven turbulence in slab geometry when a model of bootstrap current is included [53]. The NTM excitation by drift-wave turbulence such as ITG, TEM and KBM turbulence in torus plasma is still an open problem, because magnetic stochasticity and toroidal nature of turbulence may cause difference.

5.1. Magnetic island production by turbulence

Here, we will show that the turbulence produces long wavelength magnetic islands even when TM is stable/marginally stable by numerical simulations of two-fluid equations (6)–(10) in slab plasmas [37]. That implies that the turbulence modifies the excitation threshold of magnetic islands predicted in terms of Δ' based on the conventional MHD theory [11]. It is shown that magnetic islands are excited by ITG turbulence for the magnetic field configuration that is stable to TMs $\Delta' < 0$ [37].

The conventional theory of TMs predicts that the mode is unstable when the jump of perturbed poloidal magnetic field at the neutral (rational) surface is positive $\Delta' \equiv \left[\frac{1}{\hat{\psi}}\frac{\mathrm{d}\hat{\psi}}{\mathrm{d}x}\right]_{-0}^{+0} > 0$. For instance, the stability parameter is $\Delta' = \frac{2}{L_s}(\frac{1}{kL_s} - kL_s)$ for a Harris current profile $J(x) = J_0\,\mathrm{sech}^2(x/L_s)$, and Δ' is positive (negative) for a low (high) wave-number perturbation or a thin (thick) current sheet $k < 1/L_s$ ($k > 1/L_s$). We consider a sheared slab plasma, and magnetic shear length L_s is set to be large enough, so that current density gradient is small and $\Delta' < 0$, indicating that TM is stable. The ITG is set to be $\eta_i \equiv L_n/L_{Ti} \geqslant 2.5$, so that the turbulence is driven by the electromagnetic ITG mode. Parameters are set to be $\beta = 0.01$, $L/\rho_i = 80$, and $\eta = 2.35 \times 10^{-5}$. In the quasi-steady turbulent state of the ITG turbulence, magnetic islands appear on the neutral (rational) surface for the marginally stable case $\Delta' = 0$ (figure 16). Figure 17 shows the produced island width as a function of the TM stability parameter Δ'. The island width decreases with decreasing Δ' in $\Delta' > 0$ regime, however, the island width W is finite even in $\Delta' \leqslant 0$ regime [37]. This implies that magnetic islands appear even when there is no spontaneous magnetic reconnection, i.e. TMs are stable. The width of the island caused by the ITG turbulence is as large as five times of the Larmor radius (figure 17). Hence, the turbulence modifies the threshold of magnetic island appearance predicted by the conventional resistive MHD analysis in terms of Δ'.

Next, we investigate the mechanism of the coherent magnetic island formation. Figure 18 shows the time history of the reconnected flux $\Psi(t)$, which is the magnetic flux at the X-point and represents the island width by $W(t) = 4\sqrt{\Psi(t)L_s}$. It is noted that magnetic reconnection rate (reconnection electric field) is given by $E(t) = \mathrm{d}\Psi(t)/\mathrm{d}t$. The growth rate of the island and the saturated width of the island are enhanced by increasing the ITG parameter η_i. This suggests that the growth rate and the saturated width of magnetic islands are controlled by the amplitude of ITG turbulence. Figure 19 shows the time evolution of magnetic flux on the neutral sheet located at $x = 0$ for $\Delta' = 0$ and $\eta_i = 3.5$. The color is red (blue) around the

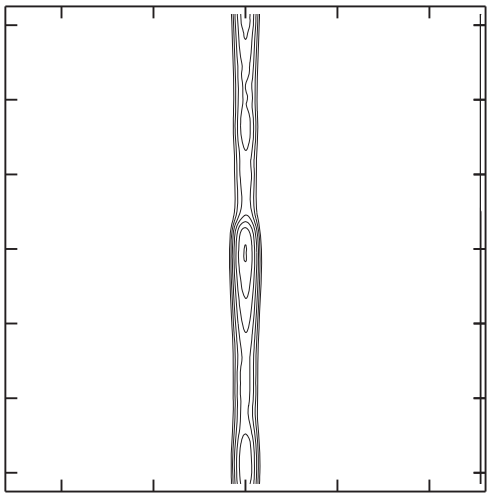

Figure 16. Equi-contours of magnetic flux representing long-wavelength magnetic islands for the marginally stable case $\Delta' = 0$.

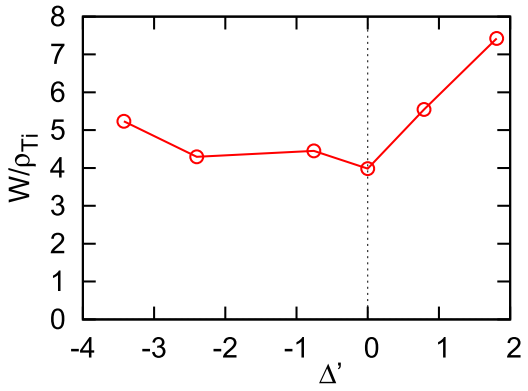

Figure 17. Magnetic island width as a function of the stability parameter of tearing mode Δ'. Reprinted from [37], with the permission of AIP Publishing.

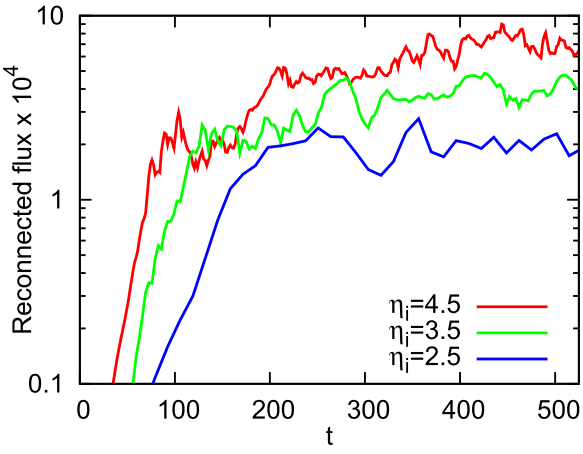

Figure 18. Time history of reconnected flux for $\Delta' = -3.4$. Reprinted from [37], with the permission of AIP Publishing.

X (O) points in figure 19(a), and the points indicate the location of the X and O points in figure 19(b). At the beginning, there are many X and O points representing small-scale magnetic islands created by magnetic reconnection driven by the

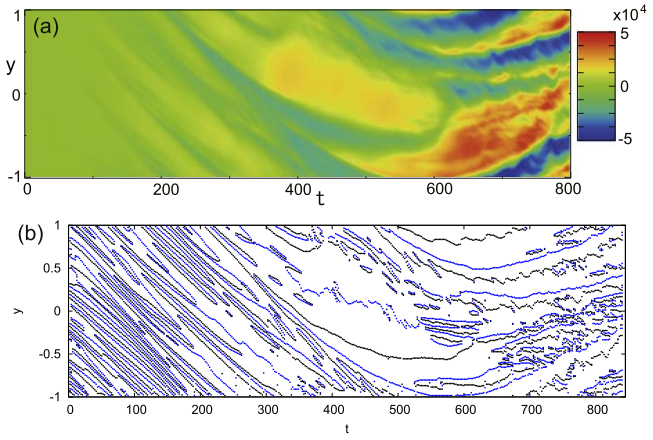

Figure 19. Time evolution of (a) magnetic flux on the neutral sheet $x = 0$, where blue region represents the core parts of magnetic islands around O-points, and (b) X-points and O-points for the case $\eta_i = 3.5$ and $\Delta' = 0$, where black points are O-points and blue points are X-points.

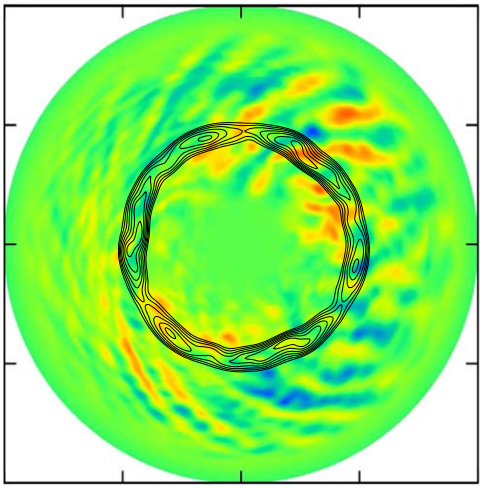

Figure 20. Color map of electrostatic potential of KBM turbulence on a poloidal section and equi-contours of helical flux that indicates magnetic islands of $m/n = 3/2$, for the case the $(m, n) = (3, 2)$ tearing mode is stable, $\Delta' \approx -2$.

electromagnetic ITG mode until $t \sim 100$. Then, the small-scale islands merge into coherent islands indicated by coherent red and blue regions appearing after $t \sim 400$. Hence, the coherent magnetic islands are produced by merging of small-scale magnetic islands produced by the ITG turbulence.

It is remarked that we have similar magnetic island production by turbulence in a torus plasmas that is unstable against micro-instabilities as shown in figure 20. The equilibrium q-profile, density profile, and temperature profile are $q = 1.05 + 2(r/\tilde{a})^2$, $n_{eq} = 0.8 + 0.2\exp[-2(r/\tilde{a})^2]$, and $T_{eq} = 0.35 + 0.65[1 - (r/\tilde{a})^2]^2$, respectively. The q-profile has a $q = 3/2$ rational surface at $r/\tilde{a} = 0.48$, and the stability parameter of TM for $(m, n) = (3, 2)$ is $\Delta' \approx -2$. It is remarked that the turbulence causes strong magnetic stochasticity around the separatrix of the islands as mentioned in section 4, so that the islands are not clear compared to those in slab plasmas.

5.2. Propagation of magnetic islands

Here, we discuss the rotation of magnetic islands in poloidal direction. Figure 19 demonstrates the reverse of propagation direction of magnetic islands. The islands propagate in the ion diamagnetic direction at the beginning because the ITG mode propagates in the ion diamagnetic direction, then the propagation direction is reversed, and they propagate in the electron diamagnetic direction. The reverse of the propagation is due to the zonal flows induced by the ITG mode. The magnetic islands control not only the propagation of magnetic perturbation of ITG turbulence but also the propagation of the resistive MHD IC [35], which is equal to the electron fluid velocity [54], and thus the direction change is generally expected. This is because the zonal flows on the neutral/rational surface have significant impact on the propagation of magnetic islands [85]. This nonlinear process is essential in reproducing the propagation velocity of the IC observed in the Large Helical Device experiment, because the linear calculations of resistive ICs do not reproduce the propagation velocity. The propagation velocity strongly depends on the island width. When the island width is small $W \ll \rho_i$, the islands propagate with the same frequency as the real-frequency of the instability producing the islands. When the island width becomes finite $W \approx \rho_i$, then the island propagates with electron fluid velocity $\mathbf{V}_{\rm island} = \mathbf{V}_e = \mathbf{V}_{E\times B} + \mathbf{V}_{*e}$ as shown in figure 14 of [54]. When the island width becomes large $W \gg \rho_i$, then the propagation velocity is the same as the zonal flow velocity $\mathbf{V}_{\rm island} = \mathbf{V}_e = \mathbf{V}_{E\times B}$ as expected from the MHD theory which is valid in the wide island limit $W \gg \rho_i$.

5.3. Nonlinear parity mixture

Let us discuss nonlinear parity mixture which is responsible for magnetic island formation by turbulence, that is pointed out in [26]. There are two types of magnetic island formation by parity mixture: the direct nonlinear mixture and a modulational instability [54]. These two types correspond to the two types of zonal flow production mechanisms by turbulence [86]. The growth rate is twice of the micro-instability $\gamma_{\rm island} \propto 2\gamma_{\rm tur}$ for the former case, while the growth rate is proportional to the saturated amplitude of micro-turbulence $\gamma_{\rm island} \propto |\Phi_{\rm tur}|$ for the latter case.

5.3.1. Direct nonlinear parity mixture. First, we describe the direct nonlinear production of tearing parity mode from the twisting parity mode which is referred to as interchange parity mode in [54]. We can divide the electrostatic potential ϕ, the magnetic flux function ψ, the electron density n, the parallel velocity $v_\parallel$, and the ion temperature T_i into the twisting and tearing parity parts $\phi = \phi_+ + \phi_-$, $\psi = \psi_+ + \psi_-$, $n = n_+ + n_-$, $v_\parallel = v_{\parallel+} + v_{\parallel-}$, and $T_i = T_{i+} + T_{i-}$, respectively, where $f_\pm$ is defined by equation (22). The twisting parity mode is represented by a set of $(\phi_+, \psi_-, n_+, v_{\parallel-}, T_{i+})$, while the tearing parity mode is denoted by a set of $(\phi_-, \psi_+, n_-, v_{\parallel+}, T_{i-})$. The nonlinear two-fluid equations for the tearing and twisting parity modes are obtained by applying the operator $\frac{1}{2}(1 \pm \mathcal{P}_x)$ to equations (12)–(16) and using equation (22) as

$$\frac{\partial \nabla^2\phi_-}{\partial t} = -[\phi_-, \nabla^2\phi_-] - [\phi_+, \nabla^2\phi_+] + [\psi_-, \nabla^2\psi_-] + [\psi_+, \nabla^2\psi_+] - d_i\beta\nabla\cdot[\nabla\phi_-, p_{i-}] - d_i\beta\nabla\cdot[\nabla\phi_+, p_{i+}], \tag{39}$$

$$\frac{\partial n_-}{\partial t} = -[\phi_-, n_-] - [\phi_+, n_+] + [\psi_-, v_{\parallel-} + d_i\nabla^2\psi_-] + [\psi_+, v_{\parallel+} + d_i\nabla^2\psi_+], \tag{40}$$

$$\frac{\partial v_{\parallel+}}{\partial t} = -[\phi_-, v_{\parallel+}] - [\phi_+, v_{\parallel-}] + \beta[\psi_-, p_+] + \beta[\psi_+, p_-], \tag{41}$$

$$\frac{\partial \psi_+}{\partial t} = -[\phi_-, \psi_+] - [\phi_+, \psi_-] - d_i\beta[\psi_-, p_{e+}] - d_i\beta[\psi_+, p_{e-}], \tag{42}$$

$$\frac{\partial T_{i-}}{\partial t} = -[\phi_-, T_{i-}] - [\phi_+, T_{i+}] - (\gamma-1)[\psi_-, v_{\parallel-}] - (\gamma-1)[\psi_+, v_{\parallel+}], \tag{43}$$

$$\frac{\partial \nabla^2\phi_+}{\partial t} = -[\phi_-, \nabla^2\phi_+] - [\phi_+, \nabla^2\phi_-] + [\psi_-, \nabla^2\psi_+] + [\psi_+, \nabla^2\psi_-] - d_i\beta\nabla\cdot[\nabla\phi_-, p_{i+}] - d_i\beta\nabla\cdot[\nabla\phi_+, p_{i-}], \tag{44}$$

$$\frac{\partial n_+}{\partial t} = -[\phi_-, n_+] - [\phi_+, n_-] + [\psi_-, v_{\parallel+} + d_i\nabla^2\psi_+] + [\psi_+, v_{\parallel-} + d_i\nabla^2\psi_-], \tag{45}$$

$$\frac{\partial v_{\parallel-}}{\partial t} = -[\phi_-, v_{\parallel+}] - [\phi_+, v_{\parallel+}] + \beta[\psi_-, p_-] + \beta[\psi_+, p_+], \tag{46}$$

$$\frac{\partial \psi_-}{\partial t} = -[\phi_-, \psi_-] - [\phi_+, \psi_+] - d_i\beta[\psi_-, p_{e-}] - d_i\beta[\psi_+, p_{e+}], \tag{47}$$

$$\frac{\partial T_{i+}}{\partial t} = -[\phi_-, T_{i+}] - [\phi_+, T_{i-}] - (\gamma-1)[\psi_-, v_{\parallel+}] - (\gamma-1)[\psi_+, v_{\parallel-}], \tag{48}$$

where the linear terms are omitted because they are the same as the r.h.s of equations (17)–(21) and conserve the parity as shown in section 3. Equations (39)–(43) imply that nonlinear interaction between the same parity modes produces the tearing parity modes $(\phi_-, \psi_+, n_-, v_{\parallel+}, T_{i-})$, and thus the tearing parity modes satisfy the nonlinear equations as shown in section 3. Hence, the tearing parity is conserved when the initial state includes only tearing parity modes as shown by many nonlinear simulations of TMs. On the other hand, the twisting parity modes $(\phi_+, \psi_-, n_+, v_{\parallel-}, T_{i+})$ are produced by the nonlinear coupling between the opposite parity modes such as $[\phi_+, \nabla^2\phi_-]$ in equations (44)–(48), and thus pure twisting parity mode does not satisfy the nonlinear equations

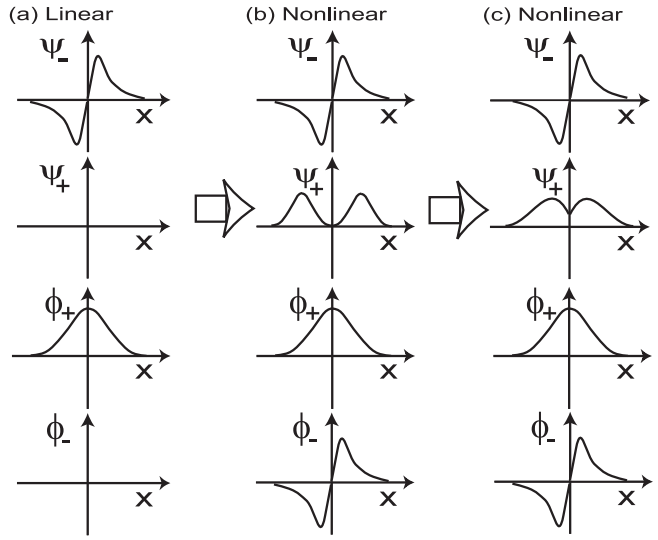

Figure 21. Magnetic island production process from twisting parity mode by nonlinear parity mixing. (a) Linear growth of perturbed magnetic flux $\psi_-$and electrostatic perturbation ϕ_+ of a twisting mode. (b) Tearing parity mode (ψ_+ , ϕ_-) production by nonlinear parity mixing. (c) The magnetic flux ψ_+ becomes finite at the resonant surface $x = 0$ implying magnetic reconnection, i.e. the production of magnetic islands.

as shown in section 3. Hence, twisting parity is not conserved when the amplitude of the instability becomes large and nonlinearity is prominent, and then the energy of the twisting parity mode is transferred into tearing parity modes. This process of tearing parity mode excitation is clearly shown by nonlinear coupling between the twisting parity modes such as $[\phi_-, \nabla^2\phi_-]$ and $[\psi_+, \nabla^2\psi_+]$ terms in the equations of tearing parity modes equations (39)–(43). Hence, magnetic islands, which have tearing parity, are produced by turbulence, which normally has twisting parity, through nonlinear parity mixture. To be precise the production of tearing parity mode does not mean the appearance of magnetic islands as described in figure 21. The excited magnetic flux of tearing parity mode vanishes at the rational surface $\psi(x = 0) = 0$ at the beginning (figure 21(b)). Then, the magnetic islands appear when magnetic reconnection takes place, i.e. the magnetic flux at $x = 0$ becomes finite $\psi(x = 0) \neq 0$ by reconnection electric field produced by forced magnetic reconnection $E_z(x = 0) = \frac{\mathrm{d}\psi(x=0)}{\mathrm{d}t} \neq 0$ (b) $\rightarrow$ (c).

5.3.2. Modulational parity instability. We have seen that the nonlinearity of turbulence mixes the parities to produce magnetic islands. Next, we present the modulational instability analysis of magnetic island formation by turbulence. The analysis is similar to the modulational instability analysis of zonal flow production by turbulence [86]. We examine the parity mixture by nonlinear terms of two-field equations for simplicity

$$\frac{\partial \nabla^2\phi}{\partial t} + [\phi, \nabla^2\phi] = [\psi, \nabla^2\psi], \tag{49}$$

$$\frac{\partial \psi}{\partial t} + [\phi, \psi] = 0. \tag{50}$$

We consider a situation that a twisting mode (Φ_+, Ψ_-) get saturated, and the fluctuation of zonal flows ($\phi_{\mathrm{zf}+}$, $\psi_{\mathrm{zf}-}$) with twisting parity is driven by the saturated twisting mode, so that $\phi = \Phi_+ + \phi_{\mathrm{zf}+} + \phi_{\mathrm{sb}-}$ and $\psi = \Psi_- + \psi_{\mathrm{zf}-} + \psi_{\mathrm{sb}+}$, where ($\phi_{\mathrm{sb}-}$, $\psi_{\mathrm{sb}+}$) is the side-band mode with tearing parity. The equations for the zonal flow and the side-band modes are obtained by assuming that they are much smaller than the saturated twisting parity mode (Φ_+, Ψ_-) $\gg$ ($\phi_{\mathrm{zf}+}$, $\psi_{\mathrm{zf}-}$), ($\phi_{\mathrm{sb}-}$, $\psi_{\mathrm{sb}+}$),

$$\frac{\partial^2 \nabla^2 \phi_{\ \mathrm{zf}+}}{\partial t^2} = [\Phi_+, [\Phi_+, \nabla^2 \phi_{\ \mathrm{zf}+}]], \tag{51}$$

$$\frac{\partial^2 \nabla^2 \phi_{\ \mathrm{sb}-}}{\partial t^2} = [\Phi_+, [\Phi_+, \nabla^2 \phi_{\ \mathrm{sb}-}]], \tag{52}$$

where only $[\phi, \nabla^2\phi]$ term is retained for simplicity. Equation (51) implies the modulational instability of zonal flows driven by the pump twisting mode Φ_+, while equation (52) implies the modulational instability of the side-band mode that has the same growth rate as the zonal flows. The magnetic perturbation of this side-band produces the magnetic islands because it has tearing parity $\psi_{\mathrm{sb}+}$. Hence, the magnetic islands are produced by turbulence through the modulational parity instability, and that is confirmed by numerical simulation (figure 8 of [54]). It is remarked that twisting parity modes can be produced from a saturated state of tearing parity modes through the nonlinear terms in equations (44)–(48), when the saturated state is unstable against twisting parity mode [87].

6. Static magnetic islands

A part of the influence of turbulence on the growth of magnetic islands should be attributed to the polarization current effects due to the flows produced by turbulence, because the polarization current is induced by the flow acceleration around the separatrix of a magnetic island. It is hard to distinguish the polarization current effect from other nonlinear interactions in electromagnetic simulations. We can extract the polarization current effect by means of electrostatic simulations with a static magnetic island, because we can eliminate nonlinear excitation of coherent magnetic island from turbulence through the merging of small-scale islands shown in figure 19. This method is first used in [28, 31], and it is found that the polarization current due to turbulence can destabilize magnetic islands. The simulation model is obtained by setting the magnetic field to represent a static magnetic island, and it is assumed that the magnetic field does not evolve.

6.1. Polarization current due to turbulence

In this section we consider a static magnetic island in the presence of turbulence to elucidate the polarization current effects driving the islands. First, we briefly review the

magnetic island equation, i.e. Rutherford equation, to elucidate the role of the polarization current [9, 88]. By neglecting the density, ion temperature, and parallel velocity $n = T_i = v_\parallel = 0$, the five-field equations (6)–(10) are reduced to the two-field equations, i.e. the reduced MHD equation

$$\frac{\partial \nabla^2 \phi}{\partial t} + [\phi, \nabla^2 \phi] = \nabla_\parallel J_\parallel, \tag{53}$$

$$\frac{\partial \psi}{\partial t} + \nabla_\parallel \phi = -\eta J_\parallel, \tag{54}$$

where $\nabla_\parallel f = -[\psi, f]$ and $J_\parallel \equiv -J = -\nabla^2 \psi$. The magnetic flux including a magnetic island can be written as $\psi = \frac{B_0}{2L_s} x^2 + \Psi \cos k_y y$ around a rational surface, where $k_y = 2\pi k / L_y$ and $k = 1$. We have $\nabla_\parallel J_\parallel = 0$, when the polarization terms (inertia terms), which is the left-hand side of the vorticity equation (53), is neglected. This implies that the current density is a flux function $J = J(\psi) = \langle J \rangle$, where $\langle\rangle$ denotes the average over a flux surface deformed by the magnetic island. When the inertia terms are retained, the current density deviates from the flux function

$$J = \langle J \rangle + J_{\rm pol}, \tag{55}$$

and the deviation is the polarization current. The flux averaged Ohm's law (equation (54)) leads to $\int \left\langle \frac{\partial \psi}{\partial t} \right\rangle \cos(k_y y) {\rm d}x = \eta \int (J - J_{\rm pol}) \cos(k_y y) {\rm d}x$ by using $\langle \nabla_\parallel f \rangle = -\langle [\psi, f] \rangle = 0$ and equation (55). By using the constant-ψ approximation, this equation can be written in terms of the island width $W = 4\sqrt{\Psi} L_s$ as

$$\frac{C}{\eta} \frac{{\rm d}W}{{\rm d}t} = \Delta' + \Delta_{\rm pol}, \tag{56}$$

where C is the constant caused by the average on the flux surface deformed by the island and is approximated to 0.8 [83],

$$\Delta' = \frac{1}{\Psi} \left[\frac{{\rm d}\psi}{{\rm d}x} \right]_{-W/2}^{+W/2}, \tag{57}$$

$$\Delta_{\rm pol} = \frac{-1}{\Psi L_x L_y} \int_{-L_x/2}^{L_x/2} \int_0^{L_y} J_{\rm pol} \cos(k_y y) {\rm d}x {\rm d}y, \tag{58}$$

[28, 31, 42] . In general, the vorticity equation includes terms other than inertia terms, and thus $\Delta_{\rm pol}$ is replaced by Δ which includes not only the polarization term but also the curvature term and the ion diamagnetic term in equation (6). Then, the Rutherford equation is rewritten as

$$\frac{C}{\eta} \frac{{\rm d}W}{{\rm d}t} = \Delta' + \Delta. \tag{59}$$

The first term Δ' represents the drive from an external current, while the second term is the drive from the internal current including the polarization current

$$\begin{aligned} \Delta &= \frac{-1}{\Psi L_x L_y} \int_{-L_x/2}^{L_x/2} \int_0^{L_y} J \cos(k_y y) {\rm d}x {\rm d}y \\ &= \frac{-1}{\Psi L_x L_y} \int_{-L_x/2}^{L_x/2} \int_0^{L_y} J_+ \cos(k_y y) {\rm d}x {\rm d}y. \end{aligned} \tag{60}$$

The last line implies that the twisting parity mode, i.e. pure IC, does not produce the polarization current. Hence, tearing parity fluctuations

$$J_+ = \frac{1}{\eta} ([\phi_-, \psi_+] + d_i \beta [\psi_+, p_{e+}]) \tag{61}$$

caused by nonlinear parity mixture produce the polarization current, because the turbulence is driven by IC/ITG mode that normally has the twisting parity (ϕ_+, ψ_-, n_+, $v_{\parallel -}$, T_{i+}) and the tearing parity mode (ϕ_-, ψ_+, n_-, $v_{\parallel +}$, T_{i-}) is produced by the nonlinear parity mixing. The internal drive caused by nonlinear terms such as the polarization current term and ion diamagnetic term, and by linear terms such as the curvature term. That is similar to the energy transfer to the coherent vortex flow discussed in section 4.2. The Reynolds stress $T_{{\rm R}mn}$, the ion diamagnetic term $T_{{\rm ID}mn}$, and the curvature term $T_{{\rm C}mn}$ in equation (38) correspond to the contribution of polarization current term, the ion diamagnetic term, and curvature term to the internal drive Δ, respectively. The influence of Maxwell stress $T_{{\rm M}mn}$ does not appear in Δ because we consider the electrostatic turbulence. It is noted that the influence of the magnetic field line bending term $T_{{\rm LB}mn}$ and the kink term $T_{{\rm KI}mn}$ are summarized to the drive from an external current Δ'.

The polarization current is controlled by plasma flow around the magnetic island, and thus a background flow against the static magnetic island is crucial for the evaluation of the polarization current. The background plasma flow consists of the $E \times B$ flow and ion and electron diamagnetic flows. The background diamagnetic flow is specified by the equilibrium density and temperature profiles. The background $E \times B$ flow is introduced by imposing a potential difference across the simulation region. The potential difference is proportional to the total flux of plasma $\Gamma = \int V_{E \times By} {\rm d}x$ through the simulation region because of $\mathbf{V}_{E \times B} = \mathbf{e}_z \times \nabla \phi$. The flux is parametrized by corresponding unperturbed velocity $u = \frac{\partial \phi_b}{\partial x}$, where $\phi_b = ux$ is the background electrostatic potential. The choice of unperturbed velocity u corresponds to the setting of boundary conditions on the electrostatic potential $\phi(x = -L_x/2) = 0$ and $\phi(x = L_x/2) = \phi_b$, and is linked to the magnetic island propagation in the poloidal direction.

There are two situations of the magnetic island propagation. One is the free propagation in the poloidal direction, which is normally realized in a saturated state of magnetic island growth due to a TM. Another is the forced propagation, in which the island has relative velocity against the background plasma flow. That is normally realized when magnetic islands are produced by an external applied magnetic field such as RMP. The mode locking is a transition from the free propagation to the forced propagation. These two situations are identified by electromagnetic force in the poloidal direction

$$\begin{aligned} F_y &= \frac{-1}{L_x L_y} \int_{-L_x/2}^{L_x/2} \int_0^{L_y} J \frac{\partial \psi}{\partial y} {\rm d}x {\rm d}y \\ &= \frac{k_y \Psi}{L_x L_y} \int_{-L_x/2}^{L_x/2} \int_0^{L_y} J_+ \sin(k_y y) {\rm d}x {\rm d}y. \end{aligned} \tag{62}$$

The last line implies that the twisting parity mode does not cause the electromagnetic force. Thus, tearing parity fluctuations

$J_+ = \frac{1}{\eta}([\phi_-, \psi_+] + d_i\beta[\psi_+, p_{e+}])$ generated by the nonlinear parity mixture cause the electromagnetic force, when the IC/ITG mode drive the turbulence. The forced propagation is represented by $F_y \neq 0$ in steady state, while $F_y = 0$ indicates the free propagation. The free propagation velocity of the island is the same as the $E \times B$ flow velocity for large magnetic islands $W \gg \rho_i$ [41, 78], while the propagation of small islands $W \approx \rho_i$ is significantly influenced by the diamagnetic flow. When the island is produced by turbulence, the propagation direction is reversed at nonlinear evolution as shown by figure 19 in section 5.2, that is explained by the appearance of zonal flows, i.e. the $E \times B$ flow produced by the turbulence.

6.1.1. Forced propagation. We present the electromagnetic force F_y and internal drive Δ for a static magnetic islands in sITG turbulence obtained by solving the five-field fluid equations in slab plasmas, equations (6)–(10), [42]. First, we present results for forced propagation case that corresponds to magnetic islands induced by an externally applied magnetic field such as RMP. Figure 22 shows the time averaged electromagnetic force F_y and internal drive Δ as a function of the unperturbed velocity normalized by the equilibrium electron diamagnetic velocity u/V_{*e} for a magnetic island with $W = 3.5\rho_i$ in the presence of ITG turbulence with $\eta_i = 2.5$. The results in the absence of ITG turbulence $\eta_i = \kappa = 0$ is added as a reference in the figure. The slopes of F_y for turbulent conditions are much larger than without turbulence $\eta_i = \kappa = 0$ in figure 22(a), and are almost independent on the viscosity μ. This may be interpreted that the turbulence enhances the force acting on the magnetic island in terms of anomalous viscosity that is proportional to the slope $\frac{dF_y}{du}$. Figure 22(b) shows that the amplitude of the internal drive Δ with turbulence ($\eta_i = 2.5$) is larger than without turbulence $\eta_i = \kappa = 0$. This implies that the ITG turbulence has a destabilizing effect on magnetic islands. The destabilizing effect is larger for the cases with unfavorable curvature $\kappa \neq 0$ than for the case $\kappa = 0$.

6.1.2. Freely propagating magnetic island. The natural (unforced) propagation velocity $u_{\rm free}$ is obtained from $F_y(u = u_{\rm free}) = 0$ obtained by interpolating the data in figure 22(a). It is noted that there is another way to obtain $u_{\rm free}$. The natural velocity $u_{\rm free}$ is obtained by modifying the boundary conditions on u_b at each time step of the simulation to reduce $|F_y|$, then the natural velocity should be $u_{\rm free} = -u_b$ when the electromagnetic force vanishes $|F_y| = 0$. The natural propagation velocity is significantly modified by the presence of turbulence $\eta_i \neq 0$, especially for the cases with unfavorable curvature $\kappa \neq 0$. This is because the sITG turbulence produces strong zonal flows. Figure 23 shows the slope of time averaged electromagnetic force at $u = u_{\rm free}$, $-\frac{dF_y}{du}(u = u_{\rm free})$ as a function of the viscosity μ, which is evaluated from figure 22(a). The slope of the force with the ITG turbulence weakly depends on the viscosity compared to the slope without the turbulence $\eta_i = 0$, and this suggests the turbulent diffusion of momentum. Figure 23 shows that the slope for $\mu = 0.01$ with turbulence is similar to that for $\mu = 0.2$ without turbulence, thus, as measured by the viscous force acting on the island, we see that the turbulence creates an effective turbulent momentum diffusivity of magnitude $\mu \approx 0.2[\rho_i^2 v_{Ti}/L_n]$, which corresponds to $\mu \approx 1.3 \times 10^{-5}[L_n v_A]$ in the MHD normalization.

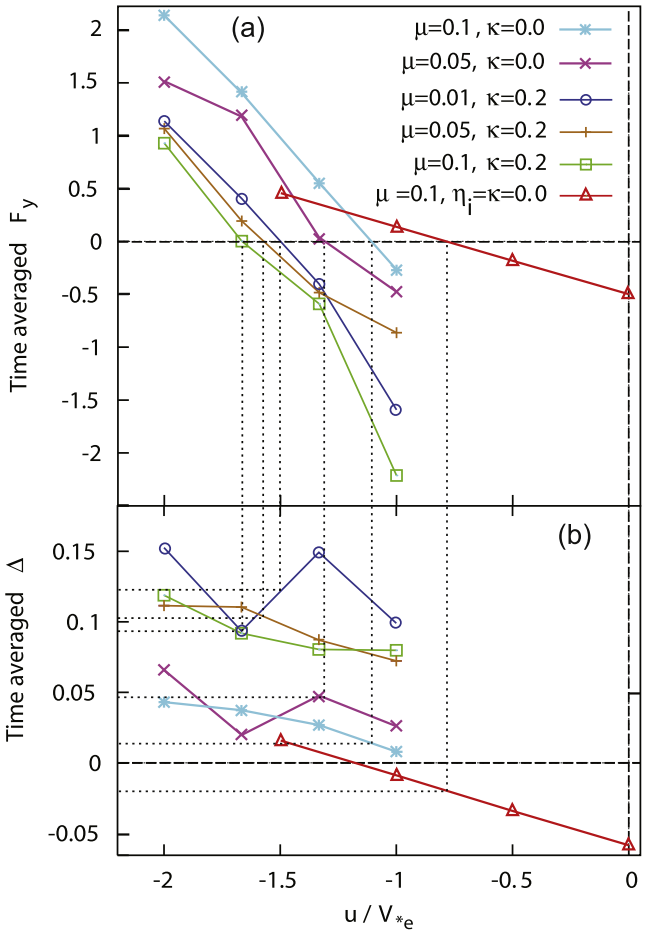

Figure 22. Comparison of the time averaged (a) electromagnetic force F_y and (b) internal drive Δ for a magnetic island with $W = 3.5\rho_i$ in the presence of ITG turbulence ($\eta_i = 2.5$) with the curvature $\kappa = 0.2$ and without the curvature $\kappa = 0$. The line labeled by $\eta_i = \kappa = 0$ represents the case without ITG turbulence. Dotted vertical (horizontal) lines indicate the values of u (Δ) for freely propagating island, and μ is the viscosity. Reprinted from [42], with the permission of AIP Publishing.

Next we present the influence of turbulence on the internal drive Δ. Figure 24 shows the internal drive term Δ as a function of the viscosity μ for a freely propagating magnetic island with the width $W = 3.5\rho_i$, which is normally realized in the mixture of turbulence and magnetic islands presented in section 5. The internal drive is negative for the case without turbulence $\kappa = \eta_i = 0$, whereas the internal drive is positive in the presence of ITG turbulence $\kappa = 0$ and $\eta_i = 2.5$. The drive is dominated by the polarization current, and therefore the polarization current due to the turbulence drives magnetic islands. Similar destabilizing effect of turbulence driven by electrostatic IC is presented by figure 17 of [31]. It is remarked that the internal drive is enhanced when we take

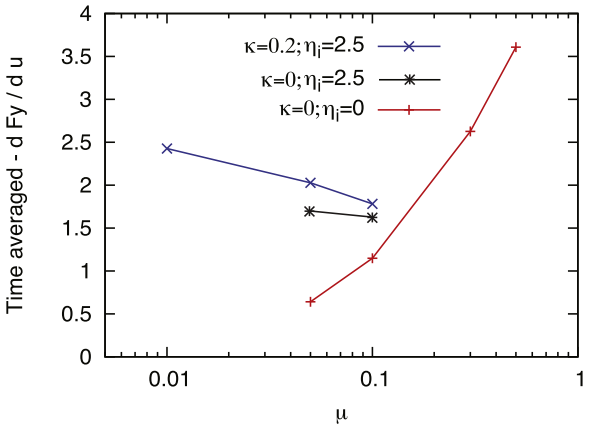

Figure 23. The slope of time averaged electromagnetic force at $u = u_{\rm free}$, $-\frac{{\rm d}F_{\rm y}}{{\rm d}u}(u = u_{\rm free})$ as a function of the viscosity μ with $W = 3.5\rho_i$ for the presence of ITG turbulence ($\eta_i = 2.5$) and the absence of ITG turbulence $\eta_i = \kappa = 0$. Reprinted from [42], with the permission of AIP Publishing.

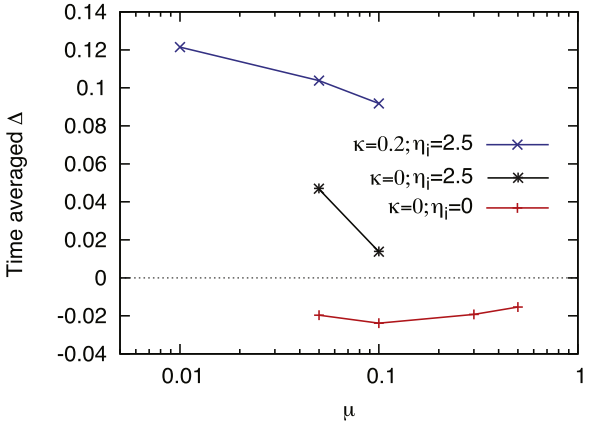

Figure 24. Time averaged internal drive Δ for freely propagating island with $W = 3.5\rho_i$ for ITG turbulence with curvature ($\eta_i = 2.5$ and $\kappa = 0.2$) for ITG turbulence without curvature ($\eta_i = 2.5$ and $\kappa = 0$), and without ITG turbulence $\eta_i = \kappa = 0$. Reprinted from [42], with the permission of AIP Publishing.

into account the Pfirsch–Schluter current due to the averaged curvature $\kappa = 0.2$.

The internal current term can be approximated by $\Delta \simeq \Delta_{\rm ITG} \equiv \frac{{\rm d}W}{{\rm d}t}|_{\eta_i \neq 0} - \frac{{\rm d}W}{{\rm d}t}|_{\eta_i = 0}$ for ITG turbulence and is evaluated numerically by assuming $\frac{{\rm d}W}{{\rm d}t}|_{\eta_i = 0} \sim \Delta'$ [43]. The magnetic island evolution with ITG turbulence $\eta_i \neq 0$ and without ITG turbulence $\eta_i = 0$ is calculated by means of electromagnetic five-field simulations, and it is found that the island is destabilized $\Delta_{\rm ITG} > 0$ for $W > 3.5\rho_i$ [43], which is consistent with the results in [41]. It is also found that the ion viscosity reduces the influence of ITG turbulence on the island [49].

6.2. Influence of island on turbulence

The influence of magnetic island on drift-wave instability is elucidated by using static islands. The problem of this analysis is that it is hard to prescribe the pressure profile, because of the lack of knowledge about the pressure profile inside the separatrix of the island. In fact, the flux-driven simulation shows that a partially but not completely flattened profile is created inside the separatrix as a result of the interaction of turbulence and islands as demonstrated in figure 14 in section 4. In addition, the flattening influences the poloidal angle dependence of turbulence intensity. The turbulence can be strong at the X point of the island [50]. The flux-driven simulation, by contrast, shows that there is little difference of the amplitude of small-scale turbulence around those points (figure 10). In numerical simulations of interactions of turbulence with magnetic islands, we normally consider two extreme pressure profiles: the completely flattened one and the one not flattened at all. When the profile is assumed not to be influenced by the appearance of the island, we use the same profile as the one without the island [32, 42, 50]. The advantage of using this profile is that we are able to directly investigate the influence of the change of magnetic field due to the island on turbulence. In these investigations it is found that magnetic islands with small width reduce the growth rate of ITG mode, while the islands with large width enhance the growth rate because of reduced magnetic shear [32]. When the profile is completely flattened inside the separatrix of magnetic island, the drift-wave instabilities are not excited inside the island. On the other hand, the gradient is enhanced just outside the separatrix, and it causes higher growth rate of micro-instability at the separatrix.

7. Summary

We have reviewed multi-scale nonlinear interactions of small-scale turbulence and large-scale magnetic islands. The interactions are especially important for understanding turbulent transport in finite beta plasmas which exhibit electromagnetic fluctuations.

The multi-scale nonlinear interactions can excite the long wavelength coherent perturbation, however, the excitation of coherent magnetic perturbation (low (m, n) modes) does not mean the production of coherent magnetic islands. Magnetic islands appear only when a coherent mode has tearing parity and magnetic reconnection takes place on a neutral/rational surface. Thus, the multi-scale interactions strongly depend on the stability of TM, which is a spontaneous magnetic reconnection and identified by the stability parameter Δ'. It is noted that we distinguish the production of finite magnetic island from a positive linear stability parameter of TM $\Delta' > 0$. The conventional linear resistive MHD stability theory of TM implies that $\Delta' > 0$ corresponds to the production of magnetic islands. On the other hand, the turbulence modifies the threshold of magnetic island appearance predicted by the conventional resistive MHD analysis in terms of Δ'. When the TM is unstable, the excited fluctuations have tearing parity, and the instability produces magnetic islands which is much wider than the Larmor radius $W \gg \rho_i$ to release the free

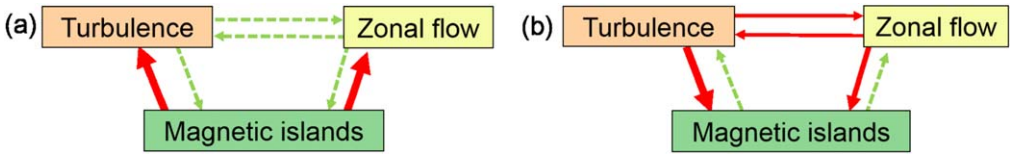

Figure 25. Multi-scale interactions among turbulence, magnetic islands, and zonal flows in cases: (a) tearing mode is unstable and (b) tearing mode is stable.

energy of equilibrium current density gradient. When the TM is stable, a part of excitation from turbulence has tearing parity and produces magnetic island on the resonant (rational) surface. The island width is several times as large as the Larmor radius $W \approx 5\rho_i$. First we summarize the former, then explain the latter.

When the TM is unstable, it causes large magnetic islands $W \gg \rho_i$, and coherent vortex flows caused by the interaction between turbulence and magnetic islands dominate turbulent fluctuations even if the growth rate of TM is smaller than drift-wave instability $\gamma_{\mathrm{TM}} \ll \gamma_{\mathrm{drift\text{-}wave}}$ (figure 9) [8, 30]. In the multi-scale interactions, magnetic islands due to TM suppress drift-wave instability by violating the ballooning structure and the spectrum of turbulence is broadened to produce the coherent vortex flows [30]. The violation of ballooning structure can be explained as follows. The drift-wave instabilities such as the ITG mode and KBM appear at the bad curvature region located at the weak field side of the torus because of the magnetic drift term $\epsilon\,[r\cos\theta, f]$ in the vorticity equation described in section 2. Magnetic islands with poloidal wavenumber m modify the parallel gradient term to $\nabla_\parallel f = \nabla_{\parallel \mathrm{eq}} f - [\Psi\cos(m\theta), f]$, where $\nabla_{\parallel \mathrm{eq}}$ is the parallel gradient in the absence of the magnetic islands, and Ψ represents the amplitude of the island by $W \propto \sqrt{\Psi}$. This implies similarity between the bad curvature region controlled by $\epsilon\,[r\cos\theta, f]$ and the island region by $[\Psi\cos(m\theta), f]$, and thus the drift-wave turbulence appearing at the bad curvature region $\cos\theta \approx 1$ can spread over the poloidal direction by the perturbed magnetic field due to the magnetic islands because $\cos m\theta \approx 1$ can be satisfied at the good curvature region. The interaction between turbulence and magnetic islands causes coherent vortex flow, which is represented by low (m, n) stable modes, inside the separatrix of the island [8, 25, 36, 55, 57, 59].The coherent vortex flow is also produced from zonal flows because the flow tends to follow the violated magnetic surfaces [8, 25, 29, 40, 59, 63]. In addition, zonal flows oscillates by the presence of the island because the influence of the island through $[\Psi\cos(m\theta), f]$ causes the magnetic island induced GAM which is corresponding to the GAM caused by the toroidicity $\epsilon\,[r\cos\theta, f]$. The magnetic field lines around the separatrix of the island is sensitive to the perturbation, and thus the stochasticity of the field lines is enhanced by turbulent fluctuations around the separatrix [30, 61]. As a result of these complicated process, total fluctuation is enhanced around the magnetic island by the nonlinear mutual interactions between turbulence and the magnetic island, and thus turbulent transport is enhanced inside the separatrix of the island. Since the coherent vortex flow and turbulence penetrate inside the magnetic islands, it causes incomplete flattening of temperature and density profiles inside the islands as observed in many numerical simulations and experiments [30, 44–46, 55, 57, 69]. The difference of turbulent fluctuation level between O and X points is small in the flux driven simulations [30], while the difference is large in non-flux driven simulations [32, 57]. From the view point of multi-scale interactions, macro-scale vortex of MHD is normally stronger than small-scale turbulence, so that macro-scale MHD dominates turbulent transport even if its growth rate is smaller than micro-turbulence (figure 25(a)). Small scale turbulence influences magnetic island growth when the island width is small and growing. The growth rate of the magnetic islands is enhanced by the anomalous current drive due to turbulence [27, 40, 50].

Even when TM is stable/marginally stable, turbulence excites long wavelength magnetic islands with the width of several times as large as the ion Larmor radius [37, 39, 47, 51–53] because turbulent fluctuations become electromagnetic at finite β. The turbulent magnetic perturbations cause magnetic reconnection, i.e. the violation of magnetic surfaces through nonlinear interactions leading to the production of magnetic islands (figure 25(b)). The excited long wavelength magnetic islands can be the seed magnetic islands of NTMs that limit the achievable β of the high-β discharge of tokamaks. This is because the NTM is a nonlinear instability and its excitation threshold island width is evaluated to be several times as large as the ion Larmor radius from experimental data [13]. The coherent islands are formed by merging of small-scale islands produced by the turbulence [37]. The detailed process of the formation of the coherent islands is divided into three steps. First is the energy transfer from high-wavenumber modes to low-wavenumber modes through nonlinear mode coupling. This excitation of the low-wavenumber modes does not mean the formation of the coherent islands. Second is the energy transfer from the twisting parity mode such as ITG, KBM, and ICs to the tearing parity mode through the nonlinear parity mixture. The third process is the magnetic reconnection that changes the topology of the magnetic field lines, then coherent magnetic islands are formed. The propagation of magnetic perturbation is changed by the appearance of magnetic islands, because the zonal flows produced by turbulence have significant influence on the propagation of the islands (figure 19) [37]. Hence, micro-turbulence influences macro-scale magnetic islands, when the plasma is stable/marginally stable to TMs. This suggests small-scale turbulence affects large-scale mode, when the larger scale mode is stable/marginally stable. That is a general feature of multi-scale interactions in magnetized

plasmas, for instance, ITG turbulence is influenced by ETG turbulence when the ITG mode is marginally stable [89].

Nonlinear parity mixture is the fundamental mechanism of magnetic island production by turbulence which has twisting parity, especially when the TM is stable [54]. The nonlinear parity mixture transfers the energy from the twisting parity mode to the tearing parity mode resulting in magnetic islands, where twisting parity modes are IC, ITG mode and KBM. The parity of the twisting parity mode is conserved during its linear growth. However, when the amplitude of the mode becomes large, the twisting parity mode does not satisfy the nonlinear two-fluid equations, while the tearing parity mode does. Thus, the nonlinear energy transfer occurs from the twisting parity mode to tearing parity modes, and then magnetic islands are produced by turbulence which has the twisting parity. The mechanism is divided into two groups: the direct excitation by nonlinear parity mixture and the modulational parity instability.

A part of the mechanism of coherent magnetic island formation by turbulence is attributed to the polarization current effect. By using the static magnetic island model in section 6, the polarization current effect is extracted from interactions between turbulence and magnetic islands. It is found that the polarization current produced by electrostatic interchange turbulence and by electrostatic sITG turbulence has destabilizing effect on the island, i.e. it drives the island [31, 42]. The effective turbulent momentum diffusivity is evaluated to be $\mu \approx 0.2[\rho_i^2 v_{Ti}/L_n]$ as measured by the viscous force acting on the island [42]. This diffusivity is important when we use turbulent viscosity to investigate the mode-locking in tokamak plasmas, and the effective viscous force is important in calculating magnetic island formation by RMPs in strong $E \times B$ flow.

Acknowledgments

This work was supported by the Japanese Ministry of Education, Culture, Sports, Science and Technology, Grant No. 17K06991.

ORCID iDs

A Ishizawa https://orcid.org/0000-0002-5323-8448

References

[1] Horton W 1999 *Rev. Mod. Phys.* **71** 735
[2] Horton W 2012 *Turbulent Transport in Magnetized Plasmas* (Singapore: World Scientific)
[3] Hahm T S and Diamond P H 2018 *J. Korean Phys. Soc.* **73** 747
[4] Diamond P H, Itoh S-I, Itoh K and Hahm T S 2005 *Plasma Phys. Control. Fusion* **47** R35
[5] Candy J 2005 *Phys. Plasmas* **12** 072307
[6] Pueschel M J, Kammerer M and Jenko F 2008 *Phys. Plasmas* **15** 102310
[7] Ishizawa A, Maeyama S, Watanabe T-H, Sugama H and Nakajima N 2015 *J. Plasma Phys.* **81** 435810203
[8] Ishizawa A and Nakajima N 2007 *Nucl. Fusion* **47** 1540
[9] Waelbroeck F L 2009 *Nucl. Fusion* **49** 104025
[10] Hender T C *et al* 2007 *Nucl. Fusion* **47** S128
[11] Furth H P, Killeen J and Rosenbluth M N 1963 *Phys. Fluids* **6** 459
[12] LaHaye R J 2006 *Phys. Plasmas* **13** 055501
[13] LaHaye R J and Sauter O 1998 *Nucl. Fusion* **38** 987
[14] Isayama A, Matsunaga G, Hirano Y and The JT-60 Team 2013 *J. Plasma Fusion Res.* **8** 1402013
[15] Evans T E *et al* 2008 *Nucl. Fusion* **48** 024002
[16] Takeji S *et al* 2002 *Nucl. Fusion* **42** 5
[17] Tanaka K *et al* 2006 *Nucl. Fusion* **46** 110
[18] Biskamp D and Welter H 1983 *Phys. Lett.* A **96** 25
[19] Diamond P H, Hazeltine R D, An Z G, Carreras B A and Hicks H R 1984 *Phys. Fluids* **27** 1449
[20] Itoh S-I, Itoh K and Yagi M 2003 *Phys. Rev. Lett.* **91** 045003
[21] Sen A, Singh R, Chandra D, Kaw P and Raju D 2009 *Nucl. Fusion* **49** 115012
[22] Itoh S-I, Itoh K and Yagi M 2004 *Plasma Phys. Control. Fusion* **46** 123
[23] McDevitt C J and Diamond P H 2006 *Phys. Plasmas* **13** 032302
[24] Yagi M, Yoshida S, Itoh S-I, Naitou H, Nagahara H, Leboeuf J-N, Itoh K, Matsumoto T, Tokuda S and Azumi M 2005 *Nucl. Fusion* **45** 900
[25] Ishizawa A and Nakajima N 2007 *Phys. Plasmas.* **14** 040702
[26] Ishizawa A and Nakajima N 2008 *Proc. 22nd IAEA Fusion Energy Conf., TH/P8-16* http://www-naweb.iaea.org/napc/physics/fec/fec2008/papers/th_p8-16.pdf
[27] Ishizawa A and Nakajima N 2008 *AIP Conf. Proc.* **1069** 110
[28] Militello F, Waelbroeck F L, Fitzpatrick R and Horton W 2008 *Phys. Plasmas* **15** 050701
[29] Li J, Kishimoto Y, Kouduki Y, Wang Z X and Janvier M 2009 *Nucl. Fusion* **49** 095007
[30] Ishizawa A and Nakajima N 2009 *Nucl. Fusion* **49** 055015
[31] Waelbroeck F L, Militello F, Fitzpatrick R and Horton W 2009 *Plasma Phys. Control. Fusion* **51** 015015
[32] Wang Z X, Li J Q, Kishimoto Y and Dong J Q 2009 *Phys. Plasmas* **16** 060703
[33] Wilson H R and Connor J W 2009 *Plasma Phys. Control. Fusion* **51** 115007
[34] Muraglia M, Agullo O, Yagi M, Benkadda S, Beyer P, Garbet X, Itoh S-I, Itoh K and Sen A 2009 *Nucl. Fusion* **49** 055016
[35] Muraglia M, Agullo O, Benkadda S, Garbet X, Beyer P and Sen A 2009 *Phys. Rev. Lett.* **103** 145001
[36] Wang Z X, Li J Q, Dong J Q and Kishimoto Y 2009 *Phys. Rev. Lett.* **103** 015004
[37] Ishizawa A and Nakajima N 2010 *Phys. Plasmas* **17** 072308
[38] Ishizawa A and Diamond P H 2010 *Phys. Plasmas* **17** 074503
[39] Muraglia M, Agullo O, Benkadda S, Yagi M, Garbet X and Sen A 2011 *Phys. Rev. Lett.* **107** 095003
[40] Li J and Kishimoto Y 2012 *Phys. Plasmas* **19** 030705
[41] Ishizawa A, Waelbroeck F L, Fitzpatrick R, Horton W and Nakajima N 2012 *Phys. Plasmas* **19** 072312
[42] Ishizawa A and Waelbroeck F L 2013 *Phys. Plasmas* **20** 122301
[43] Hu Z Q, Wang Z X, Wei L, Li J Q and Kishimoto Y 2014 *Nucl. Fusion* **54** 123018
[44] Agullo O, Muraglia M, Poye A, Benkadda S, Yagi M, Garbet X and Sen A 2014 *Phys. Plasmas* **21** 092303
[45] Hariri F, Hill P, Ottaviani M and Sarazin Y 2015 *Plasma Phys. Control. Fusion* **57** 054001
[46] Hill P, Hariri F and Ottaviani M 2015 *Phys. Plasmas* **22** 042308
[47] Poye A, Agullo O, Muraglia M, Garbet X, Benkadda S, Sen A and Dubuit N 2015 *Phys. Plasmas* **22** 030704

[48] Hu Z Q, Wang Z X, Wei L, Li J Q and Kishimoto Y 2016 *Nucl. Fusion* **56** 016012
[49] Liu T, Wang Z X, Hu Z Q, Wei L, Li J Q and Kishimoto Y 2016 *Phys. Plasmas* **23** 102508
[50] Izacard O, Holland C, James S D and Brennan D P 2016 *Phys. Plasmas* **23** 022304
[51] Agullo O, Muraglia M, Benkadda S, Poye A, Dubuit N, Garbet X and Sen A 2017 *Phys. Plasmas* **24** 042308
[52] Agullo O, Muraglia M, Benkadda S, Poye A, Dubuit N, Garbet X and Sen A 2017 *Phys. Plasmas* **24** 042309
[53] Muraglia M, Agullo O, Poye A, Benkadda S, Dubuit N, Garbet X and Sen A 2017 *Nucl. Fusion* **57** 072010
[54] Sato M and Ishizawa A 2017 *Phys. Plasmas* **24** 082501
[55] Poli E, Bottino A and Peeters A G 2009 *Nucl. Fusion* **49** 075010
[56] Poli E, Bottino A, Hornsby W A, Peeters A G, Ribeiro T, Scott B D and Siccinio M 2010 *Plasma Phys. Control. Fusion* **52** 124021
[57] Hornsby W A, Peeters A G, Snodin A P, Casson F J, Camenen Y, Szepesi G, Siccinio M and Poli E 2010 *Phys. Plasmas* **17** 092301
[58] Hornsby W A, Siccinio M, Peeters A G, Poli E, Snodin A P, Casson F J, Camenen Y and Szepesi G 2011 *Plasma Phys. Control. Fusion* **53** 054008
[59] Hornsby W A, Peeters A G, Siccinio M and Poli E 2012 *Phys. Plasmas* **19** 032308
[60] Waltz R E and Waelbroeck F L 2012 *Phys. Plasmas* **19** 032508
[61] Hornsby W A, Migliano P, Buchholz R, Zarzoso D, Casson F J, Poli E and Peeters A G 2015 *Plasma Phys. Control. Fusion* **57** 054018
[62] Hornsby W A, Migliano P, Buchholz R, Grosshauser S, Weikl A, Zarzoso D, Casson F J, Poli E and Peeters A G 2016 *Plasma Phys. Control. Fusion* **58** 014028
[63] Kwon J-M, Ku S, Choi M J, Chang C S, Hager R, Yoon E S, Lee H H and Kim H S 2018 *Phys. Plasmas* **25** 052506
[64] Ida K, Kamiya K, Isayama A, Sakamoto Y and JT-60 Team 2012 *Phys. Rev. Lett.* **109** 065001
[65] Estrada T *et al* 2007 *Nucl. Fusion* **47** 305
[66] Estrada T *et al* 2016 *Nucl. Fusion* **56** 026011
[67] Choi M J *et al* 2017 *Nucl. Fusion* **57** 126058
[68] Bardoczi L, Rhodes T L, Carter T A, Banon Navarro A, Peebles W A, Jenko F and McKee G 2016 *Phys. Rev. Lett.* **116** 215001
[69] Bardoczi L, Carter T A, La Haye R J, Rhodes T L and McKee G R 2017 *Phys. Plasmas* **24** 122503
[70] Sun P J *et al* 2012 *Phys. Scr.* **85** 055504
[71] Chen W *et al* 2017 *Nucl. Fusion* **57** 114003
[72] Sun P J *et al* 2018 *Plasma Phys. Control. Fusion* **60** 025019
[73] Sun P J *et al* (The EAST Team) 2018 *Nucl. Fusion* **58** 016003
[74] Sauter O *et al* 2010 *Plasma Phys. Control. Fusion* **52** 025002
[75] Hazeltine R D, Kotschenreuther M and Morrison P J 1985 *Phys. Fluids* **28** 2466
[76] Garbet X, Bourdelle C, Hoang G T, Maget P, Benkadda S, Beyer P, Figarella C, Voitsekovitch I, Agullo O and Bian N 2001 *Phys. Plasmas* **8** 2793
[77] Miyato N, Kishimoto Y and Li J 2004 *Phys. Plasmas* **11** 5557
[78] Fitzpatrick R, Waelbroeck F L and Militello F 2006 *Phys. Plasmas* **13** 122507
[79] Hazeltine R D and Waelbroeck F L 2004 *The Framework of Plasma Physics* (Boulder, CO: ABP Westview Press)
[80] Nishimura S, Benkadda S, Yagi M, Itoh S-I and Itoh K 2008 *Phys. Plasmas* **15** 092506
[81] Hatch D R, Pueschel M J, Jenko F, Nevins W M, Terry P W and Doerk H 2012 *Phys. Rev. Lett.* **108** 235002
[82] Bierwage A *et al* 2018 *Nat. Commun.* **9** 3282
[83] Hazeltine R D and Meiss J D 2003 *Plasma Confinement* (New York: Dover)
[84] Chen X L and Morrison P J 1990 *Phys. Fluids* B **2** 495
[85] Uzawa K, Ishizawa A and Nakajima N 2010 *Phys. Plasmas* **17** 042508
[86] Li J and Kishimoto Y 2005 *Phys. Plasmas* **12** 054505
[87] Pueschel M J, Told D, Terry P W, Jenko F, Zweibel E G, Zhdankin V and Lesch H 2014 *Astrophys. J. Suppl. Ser.* **213** 30
[88] Connor J W *et al* 2001 *Phys. Plasmas* **8** 2835
[89] Maeyama S, Idomura Y, Watanabe T-H, Nakata M, Yagi M, Miyato N, Ishizawa A and Nunami M 2015 *Phys. Rev. Lett.* **114** 255002